

# The Milky Way’s bright satellites as an apparent failure of $\Lambda$ CDM

Michael Boylan-Kolchin,<sup>\*†</sup> James S. Bullock and Manoj Kaplinghat

*Center for Cosmology, Department of Physics and Astronomy, 4129 Reines Hall, University of California, Irvine, CA 92697, USA*

27 November 2024

## ABSTRACT

We use the Aquarius simulations to show that the most massive subhalos in galaxy-mass dark matter halos in  $\Lambda$ CDM are grossly inconsistent with the dynamics of the brightest Milky Way dwarf spheroidal galaxies. While the best-fitting hosts of the dwarf spheroidals all have  $12 \lesssim V_{\max} \lesssim 25 \text{ km s}^{-1}$ ,  $\Lambda$ CDM simulations predict at least ten subhalos with  $V_{\max} > 25 \text{ km s}^{-1}$ . These subhalos are also among the most massive at earlier times, and significantly exceed the UV suppression mass back to  $z \sim 10$ . No  $\Lambda$ CDM-based model of the satellite population of the Milky Way explains this result. The problem lies in the satellites’ densities: it is straightforward to match the observed Milky Way luminosity function, but doing so requires the dwarf spheroidals to have dark matter halos that are a factor of  $\sim 5$  more massive than is observed. Independent of the difficulty in explaining the absence of these dense, massive subhalos, there is a basic tension between the derived properties of the bright Milky Way dwarf spheroidals and  $\Lambda$ CDM expectations. The inferred infall masses of these galaxies are all approximately equal and are much lower than standard  $\Lambda$ CDM predictions for systems with their luminosities. Consequently, their implied star formation efficiencies span over two orders of magnitude, from 0.2% to 20% of baryons converted into stars, in stark contrast with expectations gleaned from more massive galaxies. We explore possible solutions to these problems within the context of  $\Lambda$ CDM and find them to be unconvincing. In particular, we use controlled simulations to demonstrate that the small stellar masses of the bright dwarf spheroidals make supernova feedback an unlikely explanation for their low inferred densities.

**Key words:** dark matter – cosmology: theory – galaxies: haloes – Local Group

## 1 INTRODUCTION

It has been over ten years since it was first pointed out that the number of satellite galaxies of the Milky Way is much smaller than the number of dark matter subhalos predicted by cold dark matter (CDM)-based simulations of Milky Way-mass systems (Klypin et al. 1999; Moore et al. 1999). These subhalos formed as independent dark matter halos and were subsequently accreted onto the Milky Way’s halo, so each of them is a potential site of galaxy formation; that we only see a small number of Milky Way satellites therefore requires explanation. This discrepancy may originate from galaxies populating only a subset of the predicted subhalos, or from modifications of the CDM model on small scales such that many of these dark matter subhalos do not actually exist. Understanding which (if either) solution is correct will have vastly different implications.

In this paper, we focus on the former possibility, which associates the bright satellites of the Milky Way with the most massive subhalos expected from  $\Lambda$ CDM simulations. These models can be further split into two broad classes: those that link a satellite’s luminosity to the present day mass of its dark matter halo (Stoeckl et al. 2002; Hayashi et al. 2003; Peñarrubia et al. 2008), and those that assume satellites form only in the biggest halos defined at some earlier epoch, e.g., reionization (Bullock et al. 2000; Kravtsov et al. 2004b; Ricotti & Gnedin 2005; Koposov et al. 2009; Okamoto & Frenk 2009). Building on our recent work (Boylan-Kolchin, Bullock, & Kaplinghat 2011b) that has demonstrated a puzzling discrepancy between the masses of massive simulated subhalos and the dynamics of bright Milky Way satellites, we perform a thorough analysis of the consistency of models associating bright satellites with massive dark matter subhalos. We show that neither of these classes reconciles observations with  $\Lambda$ CDM simulations, absent further modifications: massive subhalos, defined either now or at any earlier epoch, are generically too dense to be

<sup>\*</sup> Center for Galaxy Evolution fellow

<sup>†</sup> email: m.bk@uci.edu

dynamically consistent with the Milky Way satellites. This problem relates to the structure of subhalos, making it distinct from the standard missing satellites problem, which is usually phrased in terms of abundances.

In fact, galaxy abundance issues are not limited to the Milky Way: it has been known for decades that the dark matter halo mass function has a steep low-mass slope while the faint end of the galaxy luminosity function is flat (Press & Schechter 1974; Schechter 1976), signifying a broad need for a non-linear mapping between galaxy luminosity and halo mass in cold dark matter models (e.g., White & Rees 1978). In this sense, the missing satellites problem can be interpreted as the low-luminosity manifestation of the faint galaxy issue that has been the focus of significant effort in galaxy formation theory throughout the modern era.

In recent years, many groups have shown that a simple statistical association between dark matter halos and galaxies can be used to reproduce the clustering of galaxy light and mass, and its evolution with redshift, using only dark matter structures extracted from  $N$ -body simulations (e.g., Kravtsov et al. 2004a; Conroy et al. 2006; Moster et al. 2010; Guo et al. 2010). By enforcing the cumulative abundance of galaxies to be equal to that of halos –  $n(> M_{\text{halo}}) = n(> M_*)$  – one obtains a direct galaxy-halo relation that has been tested to scales as small as  $M_{\text{halo}} \sim 5 \times 10^{10} M_{\odot}$  (Blanton et al. 2008). Abundance matching also apparently works well at reproducing the luminosity function of satellite galaxies in the Milky Way (Busha et al. 2010; Kravtsov 2010; Lunnan et al. 2012), engendering optimism that the missing satellites problem can be solved naturally in  $\Lambda$ CDM by a  $M_*(M_{\text{halo}})$  relation that falls steeply towards low halo masses. The problem would then be reduced to understanding what causes a strong suppression of galaxy formation in low-mass halos, and there are at least two well-motivated processes that likely contribute to this inefficiency.

The first crucial component is thought to be supernova feedback. If even a relatively small amount of the energy from supernovae can couple to the interstellar medium of a galaxy, it can remove gas from shallow gravitational potential wells and thereby regulate star formation in low-mass systems (Larson 1974; Dekel & Silk 1986). The second process is reionization of the Universe. After the Universe is reionized, the resultant UV background affects the gaseous content of dark matter halos both by photo-evaporation of existing gas and by suppressing subsequent accretion through an increase in the temperature of the intergalactic medium (Efsthathiou 1992; Thoul & Weinberg 1996; Barkana & Loeb 1999; Gnedin 2000; Hoeft et al. 2006; Okamoto et al. 2008). Combined, these effects reduce the baryon fraction of halos after reionization in a time-varying manner, such that more and more massive halos are affected as time progresses. Photo-heating and photo-evaporation therefore may have an important effect on galaxy formation in the host halos of the Milky Way’s dwarf galaxies (Bullock et al. 2000; Benson et al. 2002; Somerville 2002; Kravtsov et al. 2004b; Ricotti & Gnedin 2005; Madau et al. 2008b; Bovill & Ricotti 2009; Busha et al. 2010; Lunnan et al. 2012).

Semi-analytic models of galaxy formation have shown that supernova feedback and reionization should indeed strongly limit the formation of stars in low-mass halos since  $z \approx 6$  (Benson et al. 2002; Koposov et al. 2009; Muñoz et al.

2009; Li et al. 2010; Macciò et al. 2010; Guo et al. 2011; Font et al. 2011). While the detailed abundance and chemical composition of MW satellites produced in such models depends on the precise combination of reionization and supernova feedback (Font et al. 2011), it is nevertheless encouraging that such models can reproduce many properties of the MW’s satellite population using well-established physics. Models and simulations including inherently inefficient star formation (due to the difficulties in forming molecular gas in low-mass halos) have also reproduced dwarf galaxy scalings (Robertson & Kravtsov 2008; Tassis et al. 2008; Gnedin et al. 2009; Kuhlen et al. 2011). Additional feedback processes such as cosmic ray pressure may also help suppress star formation in low mass halos (Wadepuhl & Springel 2011).

In light of this substantial progress in modeling and successes in comparing observations to simulations, it is tempting to consider the  $\Lambda$ CDM model a success at reproducing the main properties of the satellite population of the Milky Way. At least one substantial issue remains, however. As we showed in a recent paper (Boylan-Kolchin, Bullock, & Kaplinghat 2011b, hereafter BBK), the majority of the most massive subhalos – the putative hosts of dwarf spheroidals – in the highest resolution  $N$ -body simulations currently available are dynamically inconsistent with all of the dSphs: massive Milky Way subhalos predicted by  $\Lambda$ CDM are too dense to host the bright MW dSphs. Considering not only the mass, but also the structure, of the dSphs’ dark matter halos provides an additional constraint beyond pure abundance matching, and shows that while abundance matching can reproduce the luminosity function of the Milky Way satellites, it does so at the expense of assigning the bright satellites to halos that are too dense to actually host the MW dSphs. This surprising result presents a new challenge for  $\Lambda$ CDM models on sub-galactic scales.

In this paper, we present a thorough comparison of the bright ( $L_V > 10^5 L_{\odot}$ ) MW dSphs and simulated MW subhalos, complementing and expanding our results in BBK. A substantial difference between BBK and this work is our treatment of subhalo mass profiles: rather than relying on mass models for the subhalos inferred from their structural properties, we use the full particle data from the numerical simulations for our comparison. Section 2 describes the observational data and numerical simulations upon which our analysis is based. We show direct comparisons of subhalo circular velocity profiles with the observed structure of Milky Way dSphs in Section 3, demonstrating that there is a significant disagreement between the two. In Section 4, we use Bayesian inference to determine the masses of the bright dSphs’ dark matter hosts and show that the results are inconsistent with any model relying on an association of the brightest satellites with the most massive dwarfs (defined at any epoch). Section 5 explores possible reasons for the mismatch between the densities of subhalos and the dynamics of dwarfs.

## 2 SIMULATIONS AND DATA

### 2.1 Simulations

Our  $\Lambda$ CDM predictions are based on dark matter halos from the Aquarius project (Springel et al. 2008), which consists

**Table 1.** Properties of the Aquarius simulations. *Columns:* (1) Simulation; (2) virial mass; and (3)–(6) number of subhalos at  $z = 0$  within 300 kpc of the halo's center and having  $V_{\text{infall}} > (20, 30, 40, 50) \text{ km s}^{-1}$ , respectively.

Name	$M_{\text{vir}} [M_{\odot}]$	$N_{20}$	$N_{30}$	$N_{40}$	$N_{50}$
Aq-A	$2.19 \times 10^{12}$	105	33	15	6
Aq-B	$9.54 \times 10^{11}$	60	16	7	1
Aq-C	$1.99 \times 10^{12}$	81	28	12	4
Aq-D	$2.19 \times 10^{12}$	111	31	15	10
Aq-E	$1.39 \times 10^{12}$	85	25	11	3
Aq-F	$1.32 \times 10^{12}$	99	29	12	5

of six Milky Way-mass dark matter halos (denoted A–F) selected at  $z = 0$  from a large cosmological simulation<sup>1</sup> and resimulated at a variety of mass and force resolutions. The specific halos selected for re-simulation were chosen at random after applying a mild isolation cut (additionally, the selected halos are predicted by a semi-analytic model to host late-type galaxies) and are generally typical of halos with similar mass (Boylan-Kolchin et al. 2010). Only halo A was simulated at the highest resolution (level 1), in which the particle mass was  $m_p = 1.7 \times 10^3 M_{\odot}$  and the Plummer equivalent gravitational softening length was  $\epsilon = 20.5 \text{ pc}$ . All halos were simulated at level 2 resolution, with  $m_p = 6.4 \times 10^3 - 1.4 \times 10^4 M_{\odot}$  and  $\epsilon = 65.8 \text{ pc}$ , resulting in approximately 120 million particles within each halo's virial radius. These six constitute our sample of simulated dark matter halos.

The masses of the Aquarius halos are  $(0.95 - 2.2) \times 10^{12} M_{\odot}$ , a range that reflects the uncertainty in the true value of the MW's virial mass and covers almost all recent estimates (see Sec. 5.1 for a more detailed discussion of various estimates of the mass of the Milky Way's dark matter halo). The exact definition of virial mass  $M_{\text{vir}}$  itself varies among different authors: it is defined to be the mass of a sphere, centered on the halo in question, containing an average density  $\Delta$  times the critical density of the Universe, but different authors adopt different values of  $\Delta$ . Throughout this paper, we use  $\Delta = \Delta_{\text{vir}}$ , the value derived from the spherical top-hat collapse model (Gunn & Gott 1972; Bryan & Norman 1998), which results in  $\Delta_{\text{vir}} \approx 94$  at  $z = 0$  for the cosmology used by the Aquarius simulations (see below).  $\Delta = 200$  and  $\Delta = 200 \Omega_m(z)$  are two other common values used in the literature.

For each halo, self-bound substructures were identified using the SUBFIND algorithm (Springel et al. 2001) as described in more detail in Springel et al. (2008). Substructures can be characterized by their total bound mass  $M_{\text{sub}}$ , or by a characteristic circular velocity  $V_{\text{max}}$ , defined to be the maximum of the circular velocity  $V_{\text{circ}} = \sqrt{GM(<r)/r}$ . We will typically use  $V_{\text{max}}$  (and  $r_{\text{max}}$ , defined as  $V_{\text{circ}}(r_{\text{max}}) = V_{\text{max}}$ ) rather than  $M_{\text{sub}}$  when discussing subhalos because  $V_{\text{max}}$  is less dependent on the specific algorithm used to identify subhalos and compute their properties.

Subhalo catalogs were constructed at each time-step for which the full particle information was saved, typically 128

snapshots per halo. The subhalos were linked across snapshots by merger trees, allowing us to explore the full evolutionary history for each subhalo in addition to its  $z = 0$  properties. Motivated by abundance matching models, we also compute the epoch  $z_{\text{infall}}$ , defined to be the redshift at which a subhalo's mass is maximized (typically just prior to infall onto a larger halo), as well as the circular velocity  $V_{\text{infall}} \equiv V_{\text{max}}(z_{\text{infall}})$  and mass  $M_{\text{infall}} \equiv M_{\text{vir}}(z_{\text{infall}})$  at that time. In each simulation, we limit our subhalo sample to those within 300 kpc of the center of the host halo and having  $V_{\text{max}}(z = 0) > 10 \text{ km s}^{-1}$ . Table 1 summarizes some important properties of the Aquarius halos and their massive subhalos.

The Aquarius simulations were performed in the context of a spatially flat WMAP1 cosmological model, with a matter density of  $\Omega_m = 0.25$ , a baryon density of  $\Omega_b = 0.045$ , reduced Hubble parameter  $h = 0.73$ , linear power spectrum normalization  $\sigma_8 = 0.9$ , and a spectral index of the primordial power spectrum of  $n_s = 1$ ; this is the same cosmology used in the Millennium and Millennium-II simulations (Springel et al. 2005; Boylan-Kolchin et al. 2009). Analysis of the WMAP7 data indicates that  $\sigma_8 = 0.81 \pm 0.03$  and  $n_s = 0.967 \pm 0.014$  (Komatsu et al. 2011, based on their “WMAP seven-year mean” values), both of which are somewhat lower than the values used in the Aquarius simulations. While reductions in these parameters may change the properties of halos predicted by  $\Lambda$ CDM, BBK showed that the Via Lactea II (VL-II) simulation (Diemand et al. 2008), which was run with  $\sigma_8 = 0.74$  and  $n_s = 0.951$ , predicts very similar structural properties of massive MW satellites to those in Aquarius. Note that the  $\sigma_8$  and  $n_s$  values of VL-II are actually lower than the WMAP7 values, which strengthens the impact of this comparison. A preliminary analysis of one MW-mass halo run using WMAP7 parameters shows that the structure of dark matter subhalos in the updated cosmology is very similar to that in the Aquarius cosmology (Garrison-Kimmel et al., in preparation). Current evidence therefore points to our results being independent of  $\sim 10\%$  changes in cosmological parameters, though it is certainly desirable to have a large sample of high resolution halos simulated in the WMAP7 cosmology in order to make the most precise predictions possible.

## 2.2 Observational data

Our primary data for each dwarf are the measured de-projected half-light radius ( $r_{1/2}$ ) and the dynamical mass within this radius ( $M_{1/2}$ ). Strigari et al. (2007a), Walker et al. (2009) and Wolf et al. (2010) have shown that the dynamical masses of the MW dSphs within a radius comparable to their stellar extent are well-constrained by kinematic data. In particular, while the radial mass profile is sensitive to factors such as the velocity anisotropy, these uncertainties are minimized at  $r_{1/2}$  (Wolf et al. 2010), resulting in a straightforward and accurate (to approximately 20%) estimate of  $M_{1/2}$ , or equivalently,  $V_{\text{circ}}(r_{1/2})$ :

$$M_{1/2} = 3 G^{-1} \langle \sigma_{\text{los}}^2 \rangle r_{1/2}, \quad (1)$$

$$V_{\text{circ}}(r_{1/2}) = \sqrt{3 \langle \sigma_{\text{los}}^2 \rangle}. \quad (2)$$

The brackets in the above equations refer to luminosity-weighted averages. While Eqn. (1) was derived using the

<sup>1</sup> This was presented in Gao et al. (2008) as the ‘hMS’ simulation, and was resimulated at  $\sim 10\times$  higher mass resolution as the Millennium-II Simulation (Boylan-Kolchin et al. 2009)

spherical Jeans equation, [Thomas et al. \(2011\)](#) have shown that this mass estimator accurately reflects the mass as derived from axisymmetric orbit superposition models as well. This result suggests that Eqns. (1) and (2) are also applicable in the absence of spherical symmetry, a conclusion that is also supported by an analysis of Via Lactea II subhalos ([Rashkov et al. 2012](#)).

We focus on the bright MW dSphs – those with  $L_V > 10^5 L_\odot$  – for several reasons. Primary among them is that these systems have the highest quality kinematic data and the largest samples of spectroscopically confirmed member stars to resolve the dynamics at  $r_{1/2}$ . The census of these bright dwarfs is also likely complete to the virial radius of the Milky Way ( $\sim 300$  kpc), with the possible exception of yet-undiscovered systems in the plane of the Galactic disk; the same can not be said for fainter systems ([Koposov et al. 2008](#); [Tollerud et al. 2008](#)). Finally, these systems all have half-light radii that can be accurately resolved with the highest resolution  $N$ -body simulations presently available.

The Milky Way contains 10 known dwarf spheroidals satisfying our luminosity cut of  $L_V > 10^5 L_\odot$ : the 9 classical (pre-SDSS) dSphs plus Canes Venatici I, which has a V-band luminosity comparable to Draco (though it is significantly more spatially extended). As in BBK, we remove the Sagittarius dwarf from our sample, as it is in the process of interacting (strongly) with the Galactic disk and is likely not an equilibrium system in the same sense as the other dSphs. Our final sample therefore contains 9 dwarf spheroidals: Fornax, Leo I, Sculptor, Leo II, Sextans, Carina, Ursa Minor, Canes Venatici I, and Draco. All of these galaxies are known to be dark matter dominated at  $r_{1/2}$  ([Mateo 1998](#)): [Wolf et al. \(2010\)](#) find that their dynamical mass-to-light ratios at  $r_{1/2}$  range from  $\sim 10 - 300$ .

The Large and Small Magellanic Clouds are dwarf irregular galaxies that are more than an order of magnitude brighter than the dwarf spheroidals. The internal dynamics of these galaxies indicate that they are also much more massive than the dwarf spheroidals:  $V_{\text{circ}}(\text{SMC}) = 50 - 60 \text{ km s}^{-1}$  ([Stanimirović et al. 2004](#); [Harris & Zaritsky 2006](#)) and  $V_{\text{circ}}(\text{LMC}) = 87 \pm 5 \text{ km s}^{-1}$  ([Olsen et al. 2011](#)). Abundance matching indicates that galaxies with luminosities equal to those of the Magellanic Clouds should have  $V_{\text{infall}} \approx 80 - 100 \text{ km s}^{-1}$  (BBK); this is strongly supported by the analysis of [Tollerud et al. \(2011\)](#). A conservative estimate of subhalos that could host Magellanic Cloud-like galaxies is therefore  $V_{\text{infall}} > 60 \text{ km s}^{-1}$  and  $V_{\text{max}} > 40 \text{ km s}^{-1}$ . As in BBK, subhalos obeying these two criteria will be considered Magellanic Cloud analogs for the rest of this work.

### 3 COMPARING $\Lambda$ CDM SUBHALOS TO MILKY WAY SATELLITES

#### 3.1 A preliminary comparison

Density and circular velocity profiles of isolated dark matter halos are well-described (on average) by [Navarro et al. \(1997, hereafter, NFW\)](#) profiles, which are specified by two parameters – i.e., virial mass and concentration, or  $V_{\text{max}}$  and  $r_{\text{max}}$ . Average dark matter subhalos are also well-fitted by NFW profiles inside of their tidal radii, though recent work has shown that the 3-parameter Einasto (1965) profile

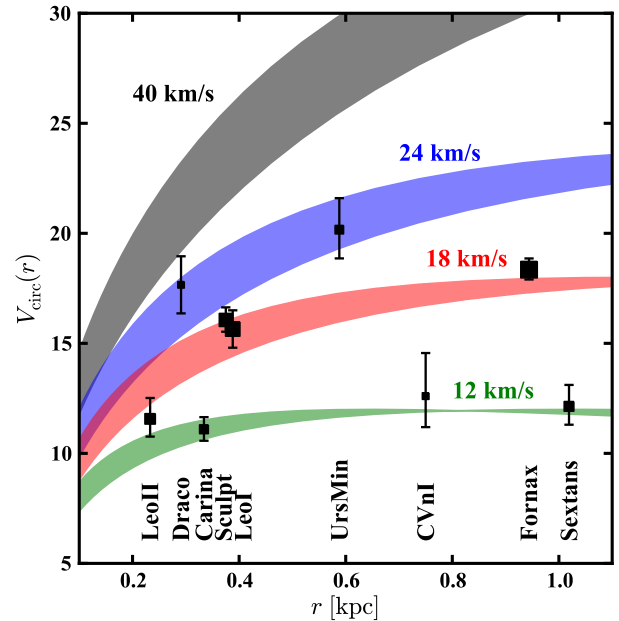


**Figure 1.** Observed  $V_{\text{circ}}$  values of the nine bright dSphs (symbols, with sizes proportional to  $\log L_V$ ), along with rotation curves corresponding to NFW subhalos with  $V_{\text{max}} = (12, 18, 24, 40) \text{ km s}^{-1}$ . The shading indicates the  $1\sigma$  scatter in  $r_{\text{max}}$  at fixed  $V_{\text{max}}$  taken from the Aquarius simulations. All of the bright dSphs are consistent with subhalos having  $V_{\text{max}} \leq 24 \text{ km s}^{-1}$ , and most require  $V_{\text{max}} \lesssim 18 \text{ km s}^{-1}$ . Only Draco, the least luminous dwarf in our sample, is consistent (within  $2\sigma$ ) with a massive CDM subhalo of  $\approx 40 \text{ km s}^{-1}$  at  $z = 0$ .

provides a somewhat better match to the profiles of both simulated halos ([Navarro et al. 2004](#); [Merritt et al. 2006](#); [Gao et al. 2008](#); [Ludlow et al. 2011](#)) and subhalos ([Springel et al. 2008](#)) even when fixing the Einasto shape parameter (thereby comparing models with two free parameters each). To connect this work to the analysis of BBK, Figure 1 compares the measured values of  $V_{\text{circ}}(r_{1/2})$  for the nine bright MW dSphs to a set of dark matter subhalo rotation curves based on NFW fits to the Aquarius subhalos; the shaded bands show the  $1\sigma$  scatter from the simulations in  $r_{\text{max}}$  at fixed  $V_{\text{max}}$ . More detailed modeling of subhalos' density profiles will be presented in subsequent sections.

It is immediately apparent that all of the bright dSphs are consistent with NFW subhalos of  $V_{\text{max}} = 12 - 24 \text{ km s}^{-1}$ , and only one dwarf (Draco) is consistent with  $V_{\text{max}} > 24 \text{ km s}^{-1}$ . Note that the size of the data points is proportional to galaxy luminosity, and no obvious trend exists between  $L$  and  $V_{\text{circ}}(r_{1/2})$  or  $V_{\text{max}}$  (see also [Strigari et al. 2008](#)). Two of the three least luminous dwarfs, Draco and Ursa Minor, are consistent with the most massive hosts, while the three most luminous dwarfs (Fornax, Leo I, and Sculptor) are consistent with hosts of intermediate mass ( $V_{\text{max}} \approx 18 - 20 \text{ km s}^{-1}$ ). Each of the Aquarius simulations contains between 10 and 24 subhalos with  $V_{\text{max}} > 25 \text{ km s}^{-1}$ , almost all of which are insufficiently massive to qualify as Magellanic Cloud analogs, indicating that models populating the most massive redshift zero subhalos with the brightest MW dwarfs will fail.



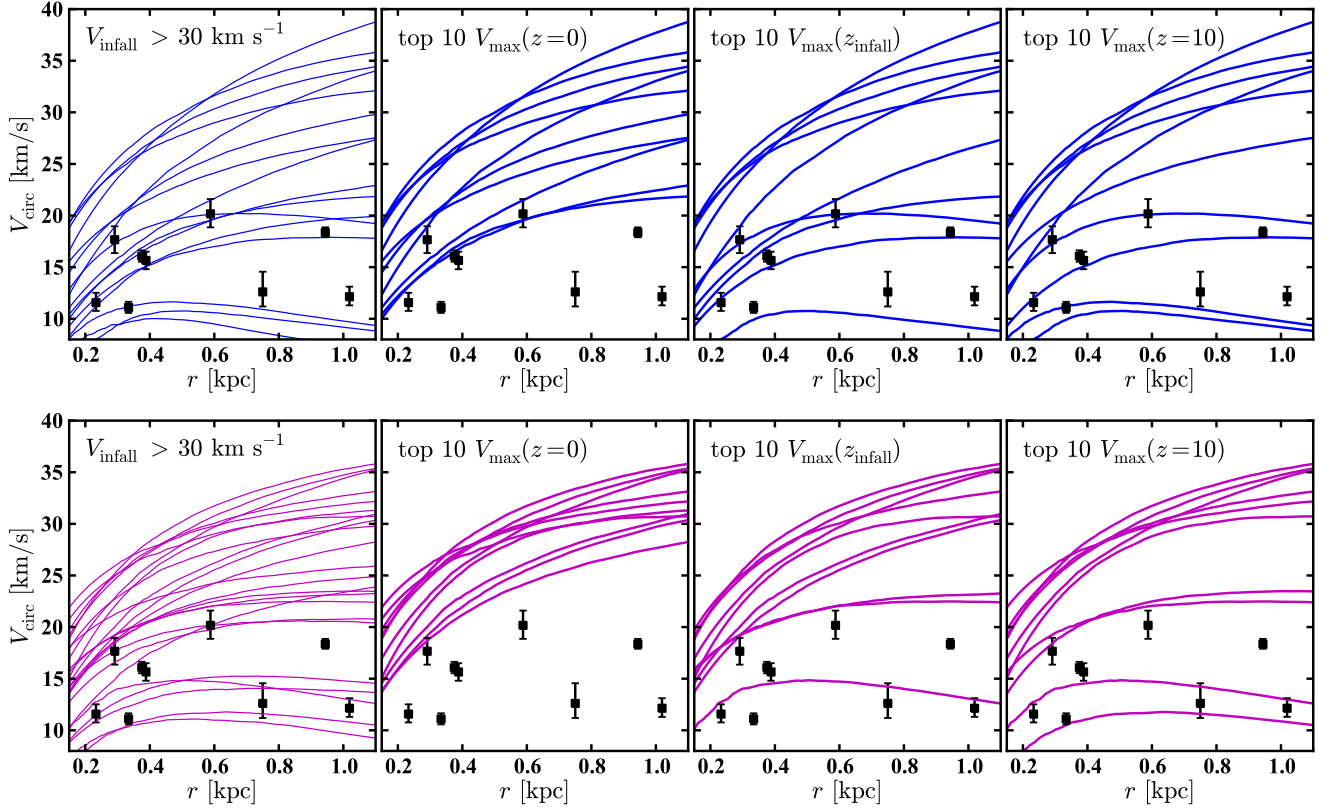


**Figure 2.** *Left panel:* circular velocity profiles at redshift zero for subhalos of the Aquarius B halo (top;  $M_{\text{vir}} = 9.5 \times 10^{11} M_{\odot}$ ) and E halo (bottom;  $M_{\text{vir}} = 1.4 \times 10^{12} M_{\odot}$ ) that have  $V_{\text{infall}} > 30 \text{ km s}^{-1}$  and  $V_{\text{max}}(z=0) > 10 \text{ km s}^{-1}$  (excluding MC candidates). Measured  $V_{\text{circ}}(r_{1/2})$  values for the MW dSphs are plotted as data points with error bars. Each subsequent panel shows redshift zero rotation curves for subhalos from the left panel with the ten highest values of  $V_{\text{max}}(z=0)$  (*second panel*),  $V_{\text{infall}}$  (*third panel*), or  $V_{\text{max}}(z=10)$  (*fourth panel*). In none of the three scenarios are the most massive subhalos dynamically consistent with the bright MW dSphs: there are always several subhalos more massive than all of the MW dSphs. (Analogous results are found for the other four halos.)

### 3.2 Assessing the consistency of massive $\Lambda$ CDM subhalos with bright Milky Way satellites

The analysis in Sec. 3.1, based on the assumption that subhalos obey NFW profiles, is similar to the analysis presented in BBK. On a case-by-case basis, however, it is possible that subhalos may deviate noticeably from NFW profiles. Consequently, *the remainder of our analysis is based on properties of subhalos computed directly from the raw particle data*. We employ a correction that takes into account the unphysical modification of the density structure of simulated subhalos due to force softening; this procedure is detailed in Appendix A. We note, however, that our results do not change qualitatively if we neglect the softening correction (see Appendix A and Table A1). By using the particle data directly, we remove any uncertainties originating from assumptions about the shape of the subhalos' density profiles.

The consistency between massive  $\Lambda$ CDM subhalos and the bright dSphs of the MW is assessed in Figure 2. As there is strong theoretical motivation to believe it is  $V_{\text{infall}}$  rather than  $V_{\text{max}}(z=0)$  that correlates with galaxy luminosity, we focus on the most massive subhalos in terms of  $V_{\text{infall}}$  – those with  $V_{\text{infall}} > 30 \text{ km s}^{-1}$ . We remove from this group all subhalos that are Magellanic Cloud analogs according to the criteria given at the end of Sec. 2.2. The left-hand panels of the figure show circular velocity profiles of the

remaining massive subhalos in two of the Aquarius halos, Aq-B (upper panels;  $M_{\text{vir}} = 9.5 \times 10^{11} M_{\odot}$ , the lowest of the Aquarius suite) and Aq-E (lower panels;  $M_{\text{vir}} = 1.39 \times 10^{12} M_{\odot}$ ). Subsequent panels show the ten most massive of these subhalos as measured at  $z=0$  (second column),  $z=V_{\text{infall}}$  (third column), and  $z=10$  (fourth column).

The most massive subhalos in terms of  $V_{\text{infall}}$  span a range of profiles at  $z=0$ , as the left panel of Fig. 2 shows. For each halo, some of these massive subhalos are consistent with the observed data while others are not. Focusing on the most massive subhalos at the present day (second panels from left), we see that these halos are markedly inconsistent with the dSphs, re-enforcing the results of Sec. 3.1. However, most subhalos that are massive at  $z=0$  were also massive in the past, a point that is emphasized in the two right panels of the figure: the bright MW dSphs are also inconsistent with either the most massive subhalos in terms of  $V_{\text{infall}}$  or those defined by their mass at  $z=10$  (a possible proxy for the mass at reionization). Even for Aq-B, the lowest mass host halo in the sample, four of the ten most massive subhalos are more massive than any of the dSphs, independent of the definition of subhalo mass.

The agreement between MW dSphs and massive subhalos is even worse for the other five Aquarius halos. In Fig. 3, we compare the redshift zero rotation curves of subhalos from each of the six Aquarius halos to the observed values

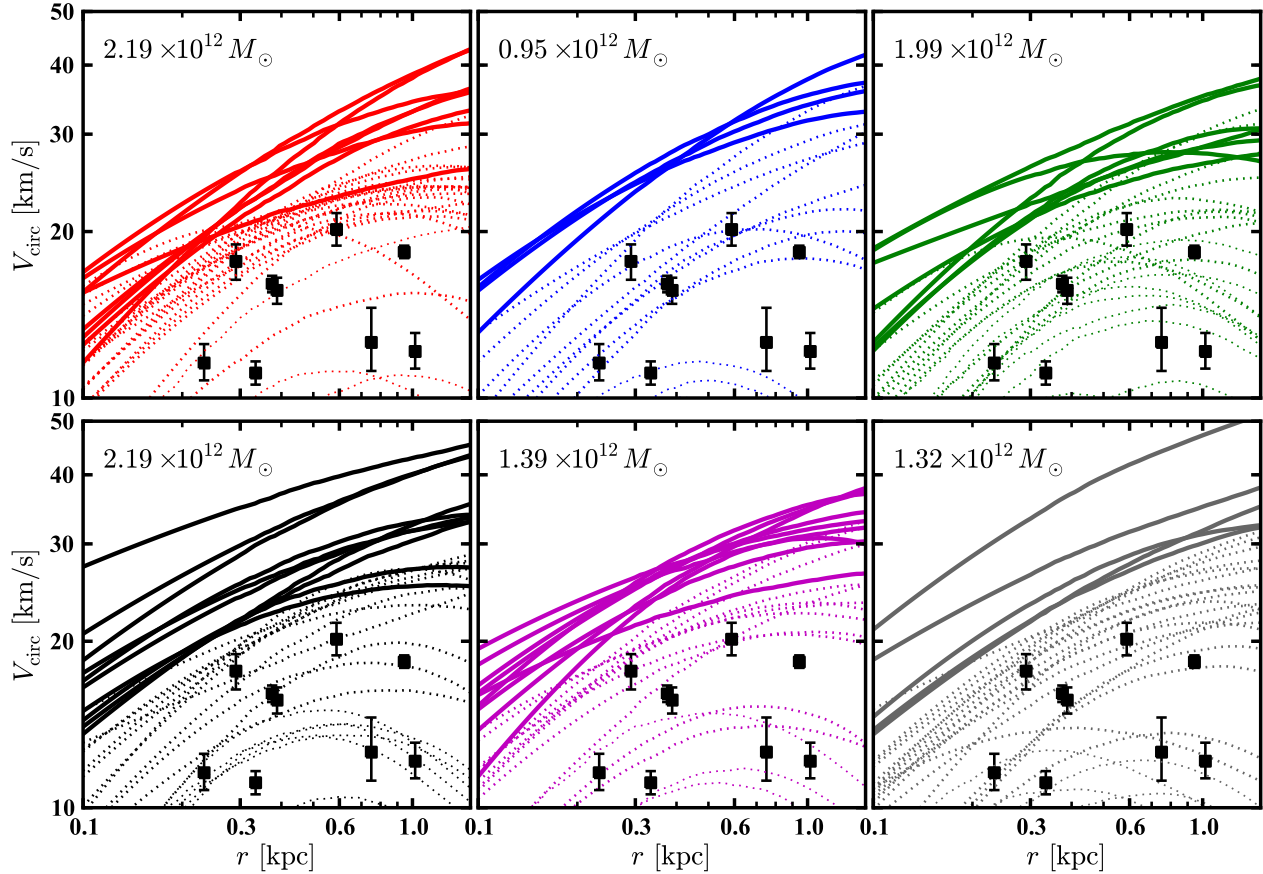


**Figure 3.** Rotation curves for all subhalos with  $V_{\text{infall}} > 30 \text{ km s}^{-1}$  and  $V_{\text{max}} > 10 \text{ km s}^{-1}$ , after excluding Magellanic Cloud analogs, in each of the six Aquarius simulations (top row, from left to right: A, B, C; bottom row: D, E, F). Subhalos that are at least  $2\sigma$  denser than every bright MW dwarf spheroidal are plotted with solid curves, while the remaining subhalos are plotted as dotted curves. Data points with errors show measured  $V_{\text{circ}}$  values for the bright MW dSphs. Not only does each halo have several subhalos that are too dense to host any of the dSphs, each halo also has several massive subhalos (nominally capable of forming stars) with  $V_{\text{circ}}$  comparable to the MW dSphs that have no bright counterpart in the MW. In total, between 7 and 22 of these massive subhalos are unaccounted for in each halo.

of  $V_{\text{circ}}(r_{1/2})$  for the bright Milky Way dwarf spheroidals. As in Fig. 2, we plot only halos with  $V_{\text{infall}} > 30 \text{ km s}^{-1}$  and  $V_{\text{max}}(z=0) > 10 \text{ km s}^{-1}$ . Subhalos that are at least  $2\sigma$  more massive than *every* dwarf (at  $r_{1/2}$ ) are plotted as solid curves; these are the “massive failures” discussed in BBK, and each halo has at least four such subhalos. Fig. 3 shows that each halo has several other subhalos with  $V_{\text{infall}} > 30$  that are unaccounted for as well: for example, halo B has three subhalos that are not massive failures by our definition but that are inconsistent at  $2\sigma$  with every dwarf except Draco. Even ignoring the subhalos that are completely unaccounted for (and are yet more massive than all of the MW dSphs), the remaining massive subhalos do not resemble the bright MW dSph population.

### 3.3 High redshift progenitors of massive subhalos

To investigate the possible impact of reionization on our results, we show the evolution of the progenitors of all subhalos with  $V_{\text{infall}} > 30 \text{ km s}^{-1}$  in Figure 4. The solid curve shows the median  $M(z)$ , while the shaded region contains 68% of the distribution, centered on the median, at each redshift.

For comparison, we also show  $T_{\text{vir}}(z) = 10^4 \text{ K}$  (the temperature at which primordial gas can cool via atomic transitions) and  $10^5 \text{ K}$  (dashed lines), as well as the mass  $M_c(z)$  below which at least half of a halo’s baryons have been removed by photo-heating from the UV background (Okamoto et al. 2008). Subhalos with  $V_{\text{infall}} > 30 \text{ km s}^{-1}$  lie above  $M_c$  and  $T_{\text{vir}} = 10^4 \text{ K}$  at all redshifts plotted, indicating that they are too massive for photo-ionization feedback to significantly alter their gas content and thereby inhibit galaxy formation.

Figure 5 focuses on the  $z=6$  properties of these subhalos. It shows the distribution of halo masses at  $z=6$  for “massive failures” (open histogram) and the remaining subhalos (filled histogram), which are possible hosts of the MW dSphs. The massive failures are more massive at  $z=6$ , on average, than the potentially luminous subhalos. This further emphasizes that reionization is not a plausible explanation of why the massive failures do not have stars: the typical massive failure is a factor of ten more massive than the UV suppression threshold at  $z=6$ . Implications of this result will be discussed in Boylan-Kolchin et al. (in preparation).

In a series of recent papers, Broderick, Chang, and

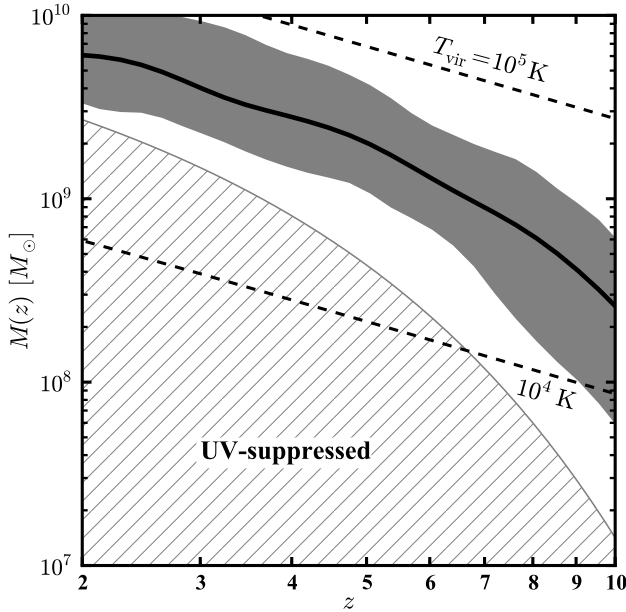


**Figure 4.** The median mass of  $z = 0$  subhalos having  $V_{\text{infall}} > 30 \text{ km s}^{-1}$  (excluding MC analogs) as function of redshift (solid curve), along with the 68% confidence range, symmetric about the median (shaded region). The hatched region marked “UV-suppressed” shows where halos are expected to have lost at least 50% of their baryonic mass owing to the UV background (Okamoto et al. 2008). Subhalos at  $z = 0$  having  $V_{\text{infall}} > 30 \text{ km s}^{-1}$  are more massive than the photo-suppression scale at all redshifts.

Pfrommer have postulated that the thermal history of the IGM at late times ( $z \lesssim 2-3$ ) could differ substantially from standard reionization models owing to a large contribution from TeV blazars. This modification relies on plasma instabilities dissipating energy from TeV blazars in the IGM, heating it to a temperature that is a factor of  $\sim 3-10$  higher than in the case of pure photo-ionization heating. Such heating would effectively increase the value of  $M_c(z)$  for  $z \lesssim 2-3$ , suppressing the stellar content of more massive halos. However, as Figure 4 shows, all halos with  $V_{\text{infall}} > 30 \text{ km s}^{-1}$  should have been able to form stars before this epoch, i.e., TeV blazar heating happens too late to kill off star formation in the Milky Way’s massive subhalos (recall that we find 16-33 subhalos with  $V_{\text{infall}} > 30 \text{ km s}^{-1}$  per halo). While TeV blazar heating therefore may help reduce the counts of void galaxies (which form later than MW subhalos) and suppress the star formation at low redshifts in progenitors of MW subhalos, it does not seem capable of explaining the structure and abundance of massive MW satellites.

#### 4 DARK MATTER MASSES OF THE MILKY WAY DWARFS

The results of Sec. 3 show that the brightest Milky Way dwarfs do not inhabit the most massive dark matter subhalos from numerical simulations. We can also use the simulations to compute the properties of subhalos that are consistent with the dynamics of the bright dSphs. These calcula-

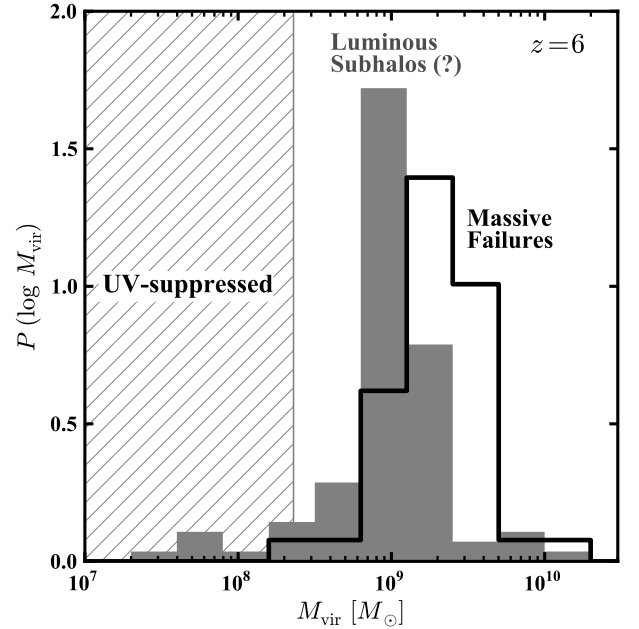


**Figure 5.** The distribution of masses at  $z = 6$  for  $z = 0$  subhalos with  $V_{\text{infall}} > 30 \text{ km s}^{-1}$  (excluding MC candidates). The open black histogram shows the “massive failures” (subhalos that are  $2\sigma$  more dense than all of the MW’s bright dSphs), while the filled gray histogram shows the remaining subhalos, which we deem to be potentially luminous satellites. Even at  $z = 6$ , the massive failures are typically more massive than subhalos consistent with the bright dSphs. They are also all more massive than characteristic scale below which the UV background significantly affects the baryon content of halos (hatched region). At  $z = 6$ , this characteristic mass is comparable to  $T_{\text{vir}} = 10^4 \text{ K}$ , the threshold for atomic cooling.

tions, and the resulting implications, are the subject of this Section.

#### 4.1 Computing properties of the dark matter hosts of the dwarf spheroidals

To compute more rigorous estimates of properties of the dSphs’ dark matter halos, we assume that the subhalo population across all six Aquarius halos forms a representative sample from  $\Lambda$ CDM simulations. We can then compute the distribution function of  $X$  (where  $X$  is, for example,  $V_{\text{max}}$ ,  $V_{\text{infall}}$ , or  $M_{\text{infall}}$ ) for a dwarf by assigning a weight (likelihood  $\mathcal{L}$ ) to each subhalo in our sample based on how closely it matches the measured  $M_{1/2}$  value of that dwarf. The posterior distribution of quantity  $X$ , given the measured value of  $M_{1/2}$  and its error  $\sigma_M$ , is given by

$$P(X|M_{1/2}, \sigma_M) \propto P(X) \mathcal{L}(X|M_{1/2}, \sigma_M). \quad (3)$$

In practice, we compute moments in the distribution of quantity  $X$  via

$$\langle X^\alpha \rangle = \frac{\sum_{i=1}^{N_{\text{subs}}} X_i^\alpha P(X_i) \mathcal{L}(X_i|M_{1/2}, \sigma_M)}{\sum_{i=1}^{N_{\text{subs}}} P(X_i) \mathcal{L}(X_i|M_{1/2}, \sigma_M)} \quad (4)$$

**Table 2.** Derived masses of the bright Milky Way dSphs. *Columns:* (1) Name of dwarf; (2) V-band luminosity (from [Wolf et al. 2010](#)); (3) median  $V_{\max}$ ; (4) median  $V_{\text{infall}}$ ; (5) median  $M_{\text{infall}}$ . The quantities in columns 3-5 are computed using Eqn. (4); the errors represent the 68.3% confidence interval.

Name	$L_V$ [ $L_\odot$ ]	$V_{\max}$ [ $\text{km s}^{-1}$ ]	$V_{\text{infall}}$ [ $\text{km s}^{-1}$ ]	$M_{\text{infall}}$ [ $M_\odot$ ]
Fornax	$1.7^{+0.5}_{-0.4} \times 10^7$	$17.8^{+0.7}_{-0.7}$	$22.0^{+4.7}_{-3.9}$	$7.4^{+6.1}_{-3.3} \times 10^8$
LeoI	$5.0^{+1.8}_{-1.3} \times 10^6$	$16.4^{+2.3}_{-2.0}$	$20.6^{+5.7}_{-4.5}$	$5.6^{+6.8}_{-3.1} \times 10^8$
Sculpt	$2.5^{+0.9}_{-0.7} \times 10^6$	$17.3^{+2.2}_{-2.0}$	$21.7^{+5.8}_{-4.6}$	$6.6^{+7.8}_{-3.6} \times 10^8$
LeoII	$7.8^{+2.5}_{-1.9} \times 10^5$	$12.8^{+2.2}_{-1.9}$	$16.0^{+4.7}_{-3.6}$	$2.4^{+3.1}_{-1.4} \times 10^8$
Sextans	$5.9^{+2.0}_{-1.4} \times 10^5$	$11.8^{+1.0}_{-0.9}$	$14.2^{+3.7}_{-2.9}$	$1.9^{+1.7}_{-0.9} \times 10^8$
Carina	$4.3^{+1.1}_{-0.9} \times 10^5$	$11.4^{+1.1}_{-1.0}$	$14.4^{+3.7}_{-3.0}$	$1.8^{+1.8}_{-0.9} \times 10^8$
UrsMin	$3.9^{+1.7}_{-1.3} \times 10^5$	$20.0^{+2.4}_{-2.2}$	$25.5^{+7.4}_{-5.8}$	$1.1^{+1.5}_{-0.6} \times 10^9$
CVnI	$2.3^{+0.4}_{-0.3} \times 10^5$	$11.8^{+1.3}_{-1.2}$	$14.5^{+4.0}_{-3.1}$	$1.9^{+2.0}_{-1.0} \times 10^8$
Draco	$2.2^{+0.7}_{-0.6} \times 10^5$	$20.5^{+4.8}_{-3.9}$	$25.9^{+8.8}_{-6.6}$	$1.2^{+2.0}_{-0.7} \times 10^9$

to compute properties of the hosts of the MW dwarf spheroidals. We assume that the likelihood functions are log-normal, and compute the relevant moments in log as well, e.g.,  $\langle \log V_{\max} \rangle$  and  $\sigma_{\log V_{\max}}^2 \equiv \langle (\log V_{\max})^2 - \langle \log V_{\max} \rangle^2 \rangle$ .

The resulting values, with  $1\sigma$  errors, for  $V_{\max}$ ,  $V_{\text{infall}}$ , and  $M_{\text{infall}}$  are listed in Table 2. This analysis confirms the preliminary comparison performed in Section 3.1. The dwarfs are all consistent with subhalos in the range of  $10 \lesssim V_{\max} \lesssim 25 \text{ km s}^{-1}$ , and at 95% confidence, *none* of the nine dwarfs have halos of  $V_{\max} = 30 \text{ km s}^{-1}$  or greater. The central values of  $V_{\text{infall}}$  range from  $\sim 14 - 26 \text{ km s}^{-1}$ , with all but Draco and Ursa Minor having  $V_{\text{infall}} < 35 \text{ km s}^{-1}$  ( $2\sigma$ ). Each simulation has 12-22 (16-33) subhalos with  $V_{\text{infall}} > 35$  (30)  $\text{km s}^{-1}$  and  $V_{\max} > 10 \text{ km s}^{-1}$ , however (the same is true for the Via Lactea II simulation: we find 27 subhalos with both  $V_{\max} > 10 \text{ km s}^{-1}$  and  $V_{\text{infall}} > 30 \text{ km s}^{-1}$ ). Even including for the Magellanic Clouds and Sagittarius, there are at least 6-21 subhalos in each simulation that are unaccounted for but have high enough masses that they should be luminous. Furthermore, the satellites predicted to be hosted by the most massive subhalos, Draco and Ursa Minor, are two of the three least luminous satellites in our sample.

Eq. (4) assumes that the probability of a subhalo hosting a specific dwarf depends only on how well that subhalo's  $M(r_{1/2, \text{dwarf}})$  agrees with the measured  $M_{1/2}$  of the dwarf. If subhalos spanning a range of  $V_{\max}$  or  $V_{\text{infall}}$  have identical values of  $M(r_{1/2, \text{dwarf}})$ , Eq. (4) assigns each of them the same probability of hosting that dwarf. In this case, the resulting mean value of  $V_{\max}$  may get larger weight from the numerous low-mass subhalos than from the less abundant high-mass subhalos since the mass function of CDM subhalos scales as  $N(> V) \propto V^{-3}$ . We have repeated our analysis with an additional weighting factor of  $V^3$  to mimic a prior of equal probability per unit log  $V$  (effectively giving massive subhalos higher weights), and find that our results are qualitatively unchanged. This is not surprising, as the data strongly constrain  $M_{1/2}$ , which, for subhalos, is tightly correlated with  $V_{\max}$ : the results are driven by the data, not by the choice of prior.

[Strigari et al. \(2007b\)](#), [Madau et al. \(2008a\)](#), and [Kuhlen \(2010\)](#) have previously used the Via Lactea simulations to derive constraints on  $V_{\max}$  (and, in the case of

[Kuhlen 2010](#),  $V_{\text{infall}}$ ) values. These were based on the masses of the satellites within either 300 or 600 pc ( $M_{300}$  or  $M_{600}$ ). Our calculations are based on a larger sample of  $\Lambda$ CDM subhalos and use more recently determined dynamical constraints on the dwarfs – the masses with their de-projected half light radii – that have smaller errors than do  $M_{300}$  or  $M_{600}$ . Furthermore, we have attempted to correct for the numerical effect of gravitational softening that affects  $M_{300}$  at the  $\sim 20\%$  level in simulations with the force resolution of Aquarius level 2. This results in a decrease in the derived  $V_{\max}$  values relative to the uncorrected case: halos of a fixed  $V_{\max}$  have larger  $M_{300}$  values after applying the correction. While our approach is somewhat more detailed than that of [Madau et al. \(2008a\)](#) and [Kuhlen \(2010\)](#), our results are generally consistent with those studies, and with [Strigari et al. \(2007b\)](#). Our results are also consistent with those of [Strigari, Frenk, & White \(2010\)](#), who have tested whether photometric and kinematic data on five of the bright dSphs are in accord with the gravitational potentials of Aquarius subhalos. They found good matches in each of the five cases, but always in systems with  $V_{\max}$  values of  $10 - 30 \text{ km s}^{-1}$ , never in more massive halos. We find somewhat smaller  $V_{\max}$  values for Draco, Leo I, Ursa Minor, and Sculptor than [Peñarrubia et al. \(2008\)](#), likely because they adopted the  $V_{\max} - r_{\max}$  relation for field dark matter halos: [Springel et al. \(2008\)](#) find that the Aquarius subhalos are systematically denser than field halos, with an offset of 0.2 dex in  $r_{\max}$  at fixed  $V_{\max}$ .

## 4.2 Comparison to $\Lambda$ CDM predictions

We are now in a position to directly compare observations and theoretical predictions for the hosts of the MW dSphs. The left-hand panel of Fig. 6 shows the luminosity functions of the Milky Way and M31 (solid black and gray curves) compared to the predicted luminosity functions from the Aquarius simulations using abundance matching, with  $M_*/L_V = 2$  (dotted curves). The abundance matching relation itself is computed by equating subhalo abundances from the Millennium and Millennium-II Simulations (closely following [Guo et al. 2010](#)) to galaxy abundances from the SDSS ([Li & White 2009](#)), with a power-law extrapolation to lower halo masses. While few of the simulated halos have subhalos massive enough to host the MW's brightest satellites, the Magellanic Clouds ([Boylan-Kolchin et al. 2010, 2011a; Busha et al. 2011](#)), the agreement on the dSph scale ( $M_V > -14$ ) is remarkably good in 5 of the 7 halos. Note that this agreement is *not* built into the abundance matching model: it results from the MW satellite luminosity function having both the same slope and amplitude as the extrapolation of the field galaxy luminosity function to (much) lower luminosities than can currently be probed statistically, which is non-trivial.

The masses of the subhalos that abundance matching predicts should host the dSphs are very different from those of the observed dSphs, however; this important point is illustrated in the right-hand panel of Fig. 6. The black squares with errors show the  $V_{\max}$  values of the MW dSphs derived in Sec. 4.1, while the magenta circles show the measured  $V_{\max}$  values from one of the numerical simulations that matches the luminosity function well (also colored magenta in the left panel of Fig. 6). The  $V_{\max}$  values of the simulated subhalos



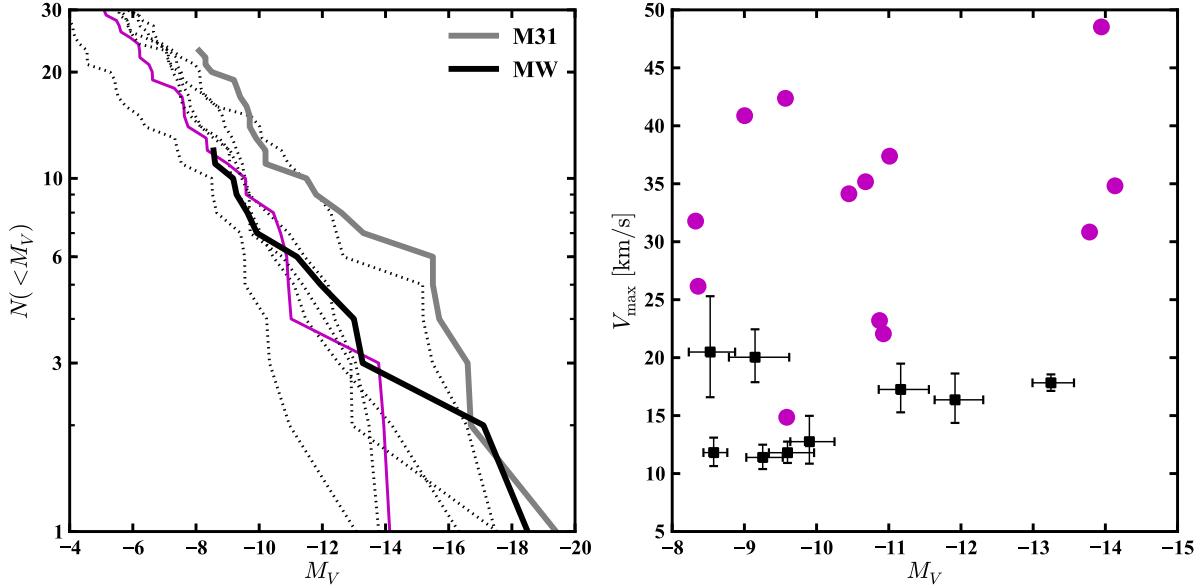


**Figure 6.** *Left:* Observed luminosity functions for the Milky Way and M31 (thick solid lines) compared to abundance matching predictions based on the Aquarius simulations (thin lines, with Aq-E plotted in magenta;  $M_*/L_V = 2$  is assumed). *Right:* Values of  $V_{\max}$  computed in Sec. 4.1 for the nine luminous Milky Way dwarf spheroidals (square symbols with errors), along with  $V_{\max}(z = 0)$  values of the subhalos with  $M_V < -8$  (magnitudes are assigned by abundance matching) from the halo that best reproduces the luminosity function in the left panel (Aq-E). While numerical simulations combined with abundance matching reproduces the luminosity function of MW satellites, the structure of the dwarf spheroidals hosts' in this model does not match observations: the simulated subhalos are much more massive (have larger values of  $V_{\max}$ ) than the dSphs.

are systematically higher than those of the MW dSphs. *It is therefore not possible to simultaneously match the abundance and structure of the MW dSphs in standard galaxy formation models based on dissipationless  $\Lambda$ CDM simulations.* While there are many subhalos that match the structure of the bright MW dSphs, these are *not* the subhalos that are predicted to host such galaxies in  $\Lambda$ CDM.

The observed densities of MW satellites are very difficult to reconcile with  $\Lambda$ CDM-based galaxy formation models, where the stellar content of a galaxy is strongly coupled to  $V_{\text{infall}}$ . To highlight the problem, we plot the inferred star formation efficiency –  $\epsilon_* \equiv M_*/(f_b M_{\text{infall}})$ , where  $f_b = \Omega_b/\Omega_m$  is the universal baryon fraction – as a function of  $M_{\text{infall}}$  in Fig. 7. The ellipses show  $1\sigma$  uncertainties (note that the direction of the ellipses is due to the inverse correlation between  $\epsilon_*$  and  $M_{\text{infall}}$  at fixed  $M_*$ ). This relation is well-constrained at  $z = 0$  in the context of abundance matching for  $M_* > 10^{8.3} M_\odot$  (approximately the completeness limit of the Li & White (2009) stellar mass function, corresponding to  $M_{\text{halo}} = 6 \times 10^{10} M_\odot$ ). The relation for  $M_*$  lower than the SDSS completeness limit is extrapolated using a power law (dashed portion of abundance matching lines).

The  $M_* - M_{\text{halo}}$  relation cannot be tested statistically on mass scales relevant for the dSphs at present, but it is immediately apparent that galaxy formation must proceed differently at  $M_{\text{halo}} \lesssim 10^{10} M_\odot$  than for larger systems if simulated subhalos accurately reflect the densities of the halos of dSphs as they exist in the Universe. For example, the most luminous dSph of the MW, Fornax, has an inferred star

formation efficiency of  $\epsilon_* \approx 0.2$ , a value that is approached only at the scale of MW-mass halos. Ursa Minor and Draco, which are  $\sim 40 - 80$  times less luminous than Fornax, sit in halos that are comparable or slightly more massive, and therefore have inferred efficiencies of closer to  $\epsilon_* = 0.002$ .

## 5 DISCUSSION

Sections 3 and 4 have demonstrated that the structure and abundance of bright Milky Way satellites are not consistent with populating the most massive subhalos in hosts of  $M_{\text{vir}} \approx (1 - 2) \times 10^{12} M_\odot$ . In this Section, we discuss some possible remedies for this problem, ranging from downward revisions of the MW's dark matter halo mass (Sec. 5.1) to changes to  $\Lambda$ CDM (Sec. 5.4).

### 5.1 Mass of the Milky Way

The simulated halos used in this paper range from  $M_{\text{vir}} = 9.5 \times 10^{11}$  to  $M_{\text{vir}} = 2.2 \times 10^{12} M_\odot$ . The true mass of the Milky Way is still a matter of significant uncertainty, however. The apparent lack of massive subhalos might be understandable if the Milky Way is significantly less massive than this simulated range. Here we summarize recent estimates of the Milky Way halo mass.

- *halo tracers*

Xue et al. (2008) used blue horizontal-branch stars from the Sloan Digital Sky Survey, combined with mock observations of hydrodynamical simulations of Milky Way-like galaxies, to find  $M_{\text{vir,MW}} = 1.0^{+0.3}_{-0.2} \times 10^{12} M_\odot$ , and  $M(<$

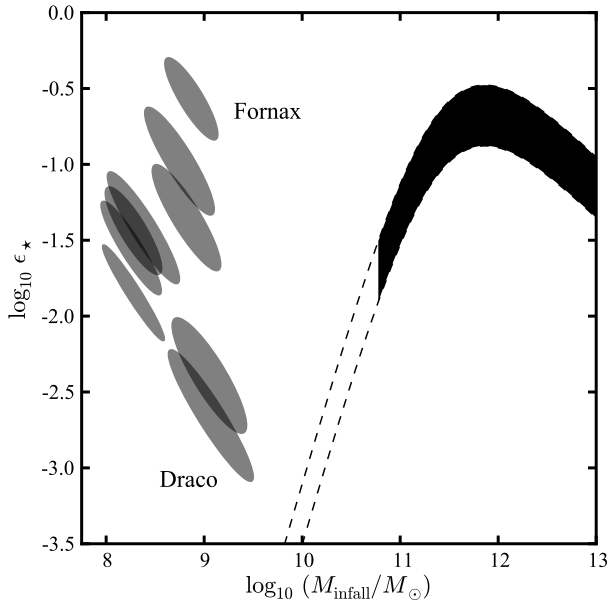


**Figure 7.** The relation between  $M_{\text{infall}}$  and star formation efficiency  $\epsilon_* = M_*/(f_b M_{\text{infall}})$ , the measure of the fraction of available baryons converted into stars in a halo. Shaded ellipses show the nine bright dSphs considered in this paper, encompassing the  $1\sigma$  uncertainties in  $M_{\text{infall}}$  from Table 2. The black shaded band and its extrapolation to lower masses (dashed lines) show  $\epsilon_*(M_{\text{infall}})$  derived from abundance matching. All of the bright dSphs have conversion efficiencies that are much higher than expected from abundance matching, given their masses. Although the dSphs have similar values of  $M_{\text{infall}}$ , their inferred conversion efficiencies vary by two orders of magnitude. At larger mass scales, this spread is closer to a factor of two at fixed  $M_{\text{infall}}$ .

60 kpc) =  $(4.0 \pm 0.7) \times 10^{11} M_\odot$ . Through a Jeans analysis of halo stars obtained from a survey for hypervelocity stars, Gnedin et al. (2010) found  $M_{\text{vir}, \text{MW}} = (1.6 \pm 0.3) \times 10^{12} M_\odot$ , and  $M(< 80 \text{ kpc}) = 6.9^{+3.0}_{-1.2} \times 10^{11} M_\odot$ . The largest uncertainties in these studies are the velocity anisotropy  $\beta$  and density profile (slope) assumed for the halo stars. Both Xue et al. (2008) and Gnedin et al. (2010) find most likely values for  $\beta$  that are near 0.4, i.e., biased toward radial orbits. A smaller value of  $\beta$  would result in increases in the mass estimates.

#### • satellite kinematics

Kinematics of satellite galaxies in the Milky Way provide constraints on its mass. These constraints are also sensitive to the assumed velocity anisotropy of the satellite population and to whether or not Leo I, which has a large line-of-sight velocity, is considered a bona fide satellite. Watkins et al. (2010) find a “best estimate” – including Leo I – of  $M(< 300 \text{ kpc}) = (2.7 \pm 0.5) \times 10^{12} M_\odot$ , which assumes that the satellite orbits are tangentially biased (based on observed proper motions); this estimate becomes  $(1.4 \pm 0.3) \times 10^{12} M_\odot$  for isotropic orbits, and  $(1.2 \pm 0.2) \times 10^{12} M_\odot$  for radially anisotropic orbits (consistent with the Xue et al. and Gnedin et al. results, which also assume such orbits).

#### • dynamics of the Large Magellanic Cloud

Measurements of the proper motion of the LMC place it at a velocity of  $\sim 360 \text{ km s}^{-1}$  (Kallivayalil et al. 2006; Piatek et al. 2008), with statistical errors of less than 5%. This

result implies that the Magellanic Clouds are likely on their first passage about the MW (Besla et al. 2007), although this conclusion may depend on the mass of the MW (Shattow & Loeb 2009). Analyses of large cosmological simulations show that objects like the LMC are extremely unlikely to be unbound to their hosts (Boylan-Kolchin et al. 2011a), which allows for estimates of the MW’s virial mass based on the dynamics of the Magellanic Clouds. Results of such estimates range from  $(1.2 - 2.0) \times 10^{12} M_\odot$ , depending on the treatment of baryonic physics and assumptions about the masses of the Clouds (Boylan-Kolchin et al. 2011a; Busha et al. 2011).

#### • masers

Masers can be used to constrain the angular speed of the local standard of rest, which, when combined with an estimate of the distance to the Galactic center, give the circular velocity of the MW at the sun’s location. Reid et al. (2009) used this technique to derive  $V = 254 \pm 16 \text{ km s}^{-1}$ , significantly higher than the IAU standard value of  $220 \text{ km s}^{-1}$  (and therefore indicating a massive dark matter halo). Ando et al. (2011) also used the maser method but found a circular velocity of  $213 \pm 5 \text{ km s}^{-1}$ , in strong disagreement with the Reid et al. value. This discrepancy is partially, but not completely, explained by different adopted distances to the Galactic Center  $R_0$ : using  $R_0 = 8.3 \text{ kpc}$  (as in Reid et al.), Ando et al.’s estimate moves to  $227 \text{ km s}^{-1}$ . A combined Bayesian analysis by Bovy et al. (2009), which incorporates maser distances but uses greater freedom in the modeling than was allowed for in either Reid et al. or Ando et al., gives  $V_c(R_0) = 236 \pm 11 \text{ km s}^{-1}$ . This is higher than, but marginally consistent with, the IAU value.

Converting between  $V_c(R_0)$  and  $M_{\text{vir}}$  is non-trivial. We can take some guidance from the MW mass models of Klypin, Zhao, & Somerville (2002), however. They found that the lowest halo mass that reasonably fit the MW was  $M_{\text{vir}} = 7.1 \times 10^{11} M_\odot$ , which gave  $V_c(R_0) = 216 \text{ km s}^{-1}$  (if angular momentum exchange between baryons and dark matter is included) or  $246 \text{ km s}^{-1}$  (without angular momentum exchange). These values require a maximal disk of  $M_* = 6 \times 10^{10} M_\odot$ , and a value of  $M(< 100 \text{ kpc}) = 3.8 \times 10^{11} M_\odot$  that is much lower than the more recent values of Gnedin et al. (2010) and McMillan (2011). The favored models of Klypin et al. (2002) assume  $M_{\text{vir}} = 1.0 \times 10^{12} M_\odot$  and  $V_{\text{max}} \approx 220 - 230 \text{ km s}^{-1}$ .

#### • other measures

McMillan (2011) adopted a Bayesian approach to constraining the mass of MW, incorporating photometric and kinematic data as well as theoretical expectations from  $\Lambda$ CDM and modeling of the Galaxy. The result was a best-fitting mass within 100 kpc of  $M(< 100 \text{ kpc}) = (0.84 \pm 0.09) \times 10^{12} M_\odot$ , and a virial mass of  $M_{\text{vir}} = (1.26 \pm 0.24) \times 10^{12} M_\odot$ . Based on abundance matching, Guo et al. (2010) found  $M_{\text{MW}} = 1.99 \times 10^{12} M_\odot$ , with an 80% confidence interval of  $(0.8 - 4.74) \times 10^{12} M_\odot$ . (These numbers are based on an overdensity criterion of  $\Delta = 200$ ; using our value of  $\Delta = 94$  moves this range to  $(0.95 - 5.7) \times 10^{12} M_\odot$ .)

The consensus of these results, then, is that the MW has a virial mass of  $\sim (1.0 - 2.0) \times 10^{12} M_\odot$ . The Aquarius halos used in this paper are broadly consistent with this range. Three of the halos – A, C, and D – lie at or slightly above  $2 \times 10^{12} M_\odot$ , while one – B – lies just below  $10^{12} M_\odot$ . That all

of these halos have a substantial population of subhalos that are unaccounted for by the bright dSphs is a strong sign that the existence of “massive failures” is not an artifact of the choice of halo masses for the Aquarius halos. Nevertheless, it is important to consider the possibility that the MW’s halo is less massive than is currently indicated by data.

The substructure abundance in within the virial radii of dark matter halos is essentially self-similar when measured in terms of  $V_{\max}/V_{\text{vir}}$  (e.g., Gao et al. 2004; De Lucia et al. 2004; van den Bosch et al. 2005; Gao et al. 2011), and the cumulative abundance of dark matter subhalos in a given halo scales as  $N(>V_{\max}) \propto V_{\max}^{-3}$  (Springel et al. 2008), so the number of halos of fixed  $V_{\max}$  will scale linearly with  $M_{\text{vir}}$ . If the Aquarius halos are more massive than the halo of the Milky Way, then our first-order expectation is that the number of subhalos that are unaccounted for by the bright MW satellites will decrease by an amount proportional to the necessary reduction in virial mass.

Since we find at least 6 subhalos with  $V_{\text{infall}} > 30 \text{ km s}^{-1}$  that are unaccounted for when  $M_{\text{vir}} = 9.5 \times 10^{11} M_{\odot}$  and 16–21 such subhalos when  $M_{\text{vir}} = 2.2 \times 10^{12} M_{\odot}$ , a reasonable scaling seems to be  $N_{\text{extra}} = 6 (M_{\text{vir}}/10^{12} M_{\odot})$ . Reducing the halo mass to  $5 \times 10^{11} M_{\odot}$  would then result in  $N_{\text{extra}} \approx 3$ , which perhaps could be explained by halo-to-halo fluctuations. However, for the Milky Way to have a virial mass of  $5 \times 10^{11} M_{\odot}$ , all of the following would need to be true: (1) the LMC, SMC, and Leo I are all unbound to the Milky Way; (2) the Magellanic Clouds are *extreme* outliers in terms of their (high) masses; (3) stars in the Galactic halo are have high (radially biased) velocity anisotropies; (4) either the Local Group has a mass that is substantially smaller than what is derived based on the timing argument (Li & White 2008), or M31 is 3–4 times more massive than the Milky Way in spite of having a fairly similar rotation velocity.

Even if this is the case, it would still not explain the gap in  $V_{\max}$  between the most massive dwarf spheroidals ( $\lesssim 25 \text{ km s}^{-1}$ ; Fig. 6, right-hand panel) and Magellanic Clouds ( $V_{\text{circ}} \gtrsim 50 \text{ km s}^{-1}$ ):  $\Lambda$ CDM simulations do not contain such a gap. We therefore believe that a downward revision of the MW’s mass is not the most likely explanation of the massive failures. As noted in Sec. 2.1, the abundance and structure of subhalos in the VL-II simulation (the only other simulation that has published data resolving subhalos on scales relevant to structure of the MW dwarfs) is very similar to that of the Aquarius simulations, providing no evidence that the background cosmology of the simulations causes the discrepancy.

Finally, in the unlikely scenario where the Milky Way’s mass has been systematically over-estimated, the unexpected span in implied star formation efficiencies demonstrated in Fig. 7 would still persist. The only way to address the massive failures problem (Figs. 2 – 6) and the efficiency problem (Fig. 7) simultaneously is to modify the inner densities of massive dark matter subhalos significantly, and in a way that is anti-correlated with stellar mass. In the next section we explore whether baryonic feedback can plausibly remedy the situation.

## 5.2 Baryonic feedback?

Energy or momentum-driven feedback from star formation is expected to drive large-scale outflows in galaxies at a va-

riety of masses and redshifts. Although this feedback cannot couple hydrodynamically to dark matter at the centers of the halos of the Milky Way dwarfs, the removal of substantial amounts of gas would cause a dynamical re-arrangement, thereby reducing the central density of dark matter. The problems discussed above may be remedied if the central regions of the rotation curves of massive subhalos can be sufficiently reduced by such blow-out. Here, we aim to estimate the magnitude of this effect due to kinetic outflows.

A supernova will release  $\sim 10^{51}$  ergs of energy into its surroundings, a fraction  $\epsilon_{\text{SN}}$  of which will couple to the gas. If we parametrize the number of supernova explosions per 100 solar masses of stars formed as  $N_{100}$ , then the gas mass carried by a supernova-driven outflow (with velocity  $V_{\text{out}}$ ) due to episode of star formation is

$$M_{\text{blow-out}} = \left[ 4 N_{100} \epsilon_{\text{SN}} \left( \frac{V_{\text{out}}}{500 \text{ km s}^{-1}} \right)^{-2} \right] M_{\star}. \quad (5)$$

The quantity in brackets is the mass-loading factor  $\eta$ , and is expected to be of order  $\eta = 1 - 2$  for energy-driven winds and  $\eta \propto V_{\max}^{-1}$  (though not exceeding  $\sim 5$ ) for momentum-driven winds (e.g., Martin 1999; Springel & Hernquist 2003; Murray et al. 2005; Davé et al. 2011).

A outflow occurring on a time scale that is short relative to a halo’s dynamical time effectively imparts an impulsive change to energy of the dark matter particles on scales small relative to the characteristic size of the pre-outflow gas distribution. We model this effect by numerically computing an isotropic, spherically symmetric equilibrium distribution function  $f(E)$  of a dark matter halo, modeled as a Hernquist (1990) profile, in the presence of a central gaseous component that is modeled as a generalized Hernquist profile (Dehnen 1993; Tremaine et al. 1994; see Boylan-Kolchin & Ma 2007 for a demonstration of the numerical stability of these models). The effect of impulsive blow-out of gas is modeled by removing the gaseous component and allowing the dark matter component to dynamically evolve to a new equilibrium in an  $N$ -body simulation. This may be viewed as an instantaneous blow-out scenario, similar to that envisioned by Navarro et al. (1996) and Read & Gilmore (2005). As our experiments do not include any contraction of the dark matter halo in response to the initial assembly of the gaseous component, they should provide upper limits on the re-arrangement of dark matter in the blow-out model. We adopt a host halo of  $V_{\max} = 35 \text{ km s}^{-1}$  with  $r_{\max} = 2 \text{ kpc}$  and investigate removing either  $2.2 \times 10^7$  or  $1.1 \times 10^8 M_{\odot}$  of gas. The scale radius of the gaseous component is set to 200 pc, and the dark matter halos are resolved with  $2 \times 10^6$  particles.

Figure 8 shows the results of these experiments. Blow-out causes an immediate drop in the gravitational potential at the system’s center. Particles with  $r \lesssim R_{\text{s,gas}}$  lose a non-negligible amount of binding energy and move to larger apocenter distances on a dynamical time-scale, while particles with pericenters  $r_p \gg R_{\text{s,gas}}$  are unaffected. The net effect is a reduction of the dark matter density for  $r \lesssim R_{\text{s,gas}}$ . Impulsively removing a gas mass of  $\sim 2 \times 10^7 M_{\odot}$  from the center of a typical  $V_{\text{infall}} = 35 \text{ km s}^{-1}$  halo has a negligible effect on the dark matter density profile (dashed line), while removing  $\sim 10^8 M_{\odot}$  of gas reduces the central  $V_{\text{circ}}$  by approximately 25%. (The inner density cusp slope, which is originally  $-1$ , ends up closer to  $-0.5$  after this

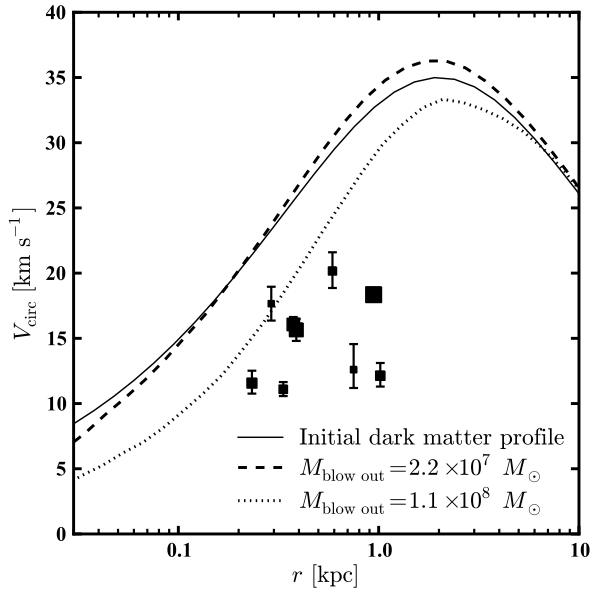


**Figure 8.** Simulations of impulsive blow-out from a  $V_{\text{max}} = 35 \text{ km s}^{-1}$  halo. The initial halo profile is plotted as a solid line; the dashed and dotted curves correspond to the final, relaxed profile after gas blow-out of  $2.2 \times 10^7$  and  $1.1 \times 10^8 M_{\odot}$ , respectively. Measured values of  $V_{\text{circ}}$  for the bright dSphs are plotted as squares, sized proportional to  $\log L_V$ , with error bars. We emphasize that the two data points closest to the halo line post-blowout are among the least luminous dwarfs we consider (Draco and Ursa Minor, with  $L_V \simeq 2 - 4 \times 10^5$ ). Matching their densities via impulsive feedback would then require ejecting  $\sim 100$  times as much mass as is present in stars today in these systems.

maximal blow-out.) This result is consistent with Navarro et al. (1996), who used numerical simulations to show that a supernova-driven outflow following a single episode of star formation that created  $\sim 10^8 M_{\odot}$  of stars can create a core in the dark matter halo of a  $V_{\text{circ}} \sim 50 \text{ km s}^{-1}$  dwarf galaxy. It also agrees with the work of Read & Gilmore (2005), which found that removing the vast majority of a dwarf galaxy’s baryons (95–99%) in either one or two impulsive episodes significantly flattens a dark matter density cusp, with two blow-outs creating a dark matter core. Gnedin & Zhao (2002) demonstrated that removal of a gaseous disk containing nearly all of a dwarf galaxy’s baryons will reduce the central dark matter density by approximately 50%; our reduction of  $\sim 25\%$  in  $V_{\text{circ}}$  is in good agreement with this result.

The final dark matter profile after removing  $10^8 M_{\odot}$  of gas agrees only with Draco among the dSphs (square symbols with error bars). Blowing out  $10^8 M_{\odot}$  of gas requires forming  $\eta^{-1} 10^8 M_{\odot}$  of stars, however [see Eqn. (5)]. Since the bright dSphs have  $M_{\star} \approx 5 \times 10^5 - 5 \times 10^7 M_{\odot}$  and  $\eta$  should be of order unity (and certainly not in excess of 10), only the brightest dSph (Fornax) has formed enough stars to remove the necessary amount of gas. In particular, the necessary amount of star formation exceeds the stellar content of Draco by a factor of  $\sim 200$ , and the reduction in density is not sufficient to match Fornax’s observed  $V_{\text{circ}}$  (the largest square, with  $V_{\text{circ}} \sim 17 \text{ km s}^{-1}$  at  $\sim 0.9 \text{ kpc}$ ).

Starting with a much more concentrated baryonic component – e.g., with a scale radius of 1–10 pc rather than 100

pc, as assumed in this work – could cause gas blow-out to have a more deleterious effect on the central region of the dark matter halo. Collecting  $10^8 M_{\odot}$  of gas in such a small region would likely steepen the initial dark matter profile a great deal, however. It would also result in star formation that is very centrally concentrated, in contrast to the typical half-light radii of the bright dwarfs of  $300 \lesssim r_{1/2} \lesssim 1000 \text{ pc}$ . If the stars are indeed formed at very small radii, they would have to migrate outward in order to match observed sizes of the dSphs, which would perhaps result in radially biased velocities in the dwarfs’ central regions. We conclude that absent outflows that are much larger than expected in usual models of galaxy formation (i.e., absent mass loading factors of  $\eta = 10 - 100$ ) or an extremely concentrated gaseous distribution, impulsive gas removal due to supernova feedback is likely insufficient to lower the central densities of the massive subhalos predicted by  $\Lambda$ CDM enough to agree with observations of the bright dSphs. In the future, it may be possible to more directly constrain the amount of mass removed from dSphs through detailed analysis of chemical abundance patterns (Kirby et al. 2011).

Governato et al. (2010) have recently performed a very high resolution simulation with a star formation density threshold of  $100 \text{ cm}^{-3}$  and found it produces a cored galaxy with  $M_{\star} = 5 \times 10^8 M_{\odot}$  in a halo of  $M_{\text{vir}} = 5.7 \times 10^{10} M_{\odot}$  ( $V_{\text{circ}} \sim 60 \text{ km s}^{-1}$ ). Pontzen & Governato (2011) argued that the effects of repeated cycles of star formation, blow-out, and re-cooling can explain these results. Unless this process is somehow much more efficient than the instantaneous blow-out scenario discussed above – i.e., unless it removes much more gas mass per stellar mass formed than does a single episode of instantaneous blow-out – it is unlikely to explain the low densities of the Milky Way dwarf spheroidals: the Governato et al. galaxy has a stellar mass that is a factor of 10 larger than any of the MW dSphs (and a factor of 1000 larger than several of the bright dSphs). High resolution hydrodynamical simulations of the Milky Way’s satellites find that the net effect of star formation and feedback is either negligible or causes an increase in the dark matter density (di Cintio et al. 2011; Parry et al. 2012). Clearly, it will be invaluable to have a larger number of simulations of possible dSphs over a wider mass range, simulated with different codes and stellar feedback prescriptions. It will also be interesting to better constrain the possible role of black hole feedback, which can power strong outflows without relying on star formation, in the Milky Way dSphs. Reines et al. (2011) have recently discovered an AGN in a dwarf starbursting galaxy with a mass similar to that of the LMC (i.e., more massive than the MW dSphs); as of yet, there is no evidence for central black holes in the dSphs, with Jardel & Gebhardt (2012) finding a  $1\sigma$  upper limit of  $3.2 \times 10^4 M_{\odot}$  for the mass of a potential black hole at the center of Fornax.

### 5.3 Stochastic galaxy formation?

If baryonic feedback has not strongly modified the structure of massive MW subhalos, and the abundance of these objects is commensurate with that found in the Aquarius simulations, then it seems unavoidable that galaxy formation must be *highly* stochastic in halos of  $\lesssim 50 \text{ km s}^{-1}$  ( $M_{\text{infall}} \lesssim 10^{10} M_{\odot}$ ). By this, we mean that the stellar mass



of a galaxy cannot correlate with its dark matter halo mass at these scales (see Fig. 7). Stochasticity is not unexpected in low halo masses, as gas cooling will depend strongly on the ability to form molecular gas, which in turn depends on the gas metallicity (Kuhlen et al. 2011). An additional source of scatter in stellar mass at fixed halo mass comes from allowing satellites to have a  $M_{\text{halo}} - M_{\star}$  relation that differs from that of central galaxies (Neistein et al. 2011). Yang et al. (2011) have demonstrated that such a variation is expected because the stellar mass of a satellite should be related to the  $M_{\text{halo}} - M_{\star}$  relation at  $z_{\text{infall}}$ , not at  $z = 0$ . (It remains to be seen whether the abundance of MW satellites is correctly reproduced in this or similar abundance matching models.)

However, the stochasticity required by the results of Table 2 and Fig. 7 is somewhat more curious: it requires a strong (and systematic) suppression of galaxy formation in the most dense subhalos of the Milky Way, which is counter-intuitive. It also requires that the luminosities of *all* subhalos with  $30 \lesssim V_{\text{max}} \lesssim 60 \text{ km s}^{-1}$  – a range in which we expect to find several objects in the Milky Way – host galaxies with luminosities a factor of 10-1000 lower than subhalos in the range  $15 \lesssim V_{\text{max}} \lesssim 30 \text{ km s}^{-1}$ . If this is due to scatter, it must be only scatter in one direction, toward low  $M_{\star}$  at fixed  $M_{\text{halo}}$ , in the mass range of massive failures, which would host galaxies with luminosities comparable to ultra-faint dwarf spheroidal galaxies in this scenario.

The dynamics of the ultra-faint are not as well constrained as those of the bright dSphs for two main reasons. First, the kinematic data for the ultra-faint galaxies of the Milky Way are not of the same quality as for the bright dSphs. Additionally, the ultra-faints have smaller half-light radii, which means that measurements of  $M_{1/2}$  have less power in constraining  $V_{\text{max}}$ . It is therefore possible that some, or all, of the massive failures are accounted for by ultra-faint galaxies; at least, this is not presently ruled out by the data. If this is the case, however, then galaxy formation must be *extremely* stochastic in halos of  $V_{\text{infall}} \lesssim 40 - 50 \text{ km s}^{-1}$ , as it would require  $M/L$  variations in excess of 1000 at this scale to simultaneously explain the ultra-faints and the brightest dSphs. As shown in Fig. 4, the massive failures are all more massive than the photo-suppression threshold at all times, so it is not clear what shuts off star formation in the massive failures hosting ultra-faints in this scenario. For example, the hybrid simulations of Bovill & Ricotti (2011a,b), which reproduce many observed properties of the ultra-faint dwarf spheroidals by placing them in halos below the filtering mass, over-produce brighter Milky Way dwarfs, even though only star formation prior to reionization is considered.

#### 5.4 Different dark matter physics on sub-galactic scales?

Should none of the explanations in Sections 5.1 - 5.3 prove correct, then modifications of the  $\Lambda$ CDM model on small scales may be necessary to explain the structure of the MW dSphs. Indeed, Lovell et al. (2012) have already examined the structure of a version of the Aquarius A halo simulated in a Warm Dark Matter cosmology. They find that WDM substantially alleviates the massive failure problem, as the subhalos in this simulation are (1) less numerous and (2) less

dense than their counterparts in the CDM run. Although this result is very promising, it remains to be seen whether WDM simulations produce *enough* substructure to account for the ultra-faint galaxies of the MW (Macciò & Fontanot 2010; Polisensky & Ricotti 2011). The particle mass used by Lovell et al. (2012) is also near the lower limit of what is allowed by observations of Lyman- $\alpha$  absorption features in the spectra of distant quasars (Boyarsky et al. 2009). Improved measurements of this type will further constrain the allowed parameter space for WDM and the viability of  $\Lambda$ WDM as a cosmological model.

Alternatively, it may be the case that dark matter is not strictly collisionless, but rather has a non-negligible cross section for self-scattering (Spergel & Steinhardt 2000). This self-interacting dark matter (SIDM) model was originally proposed to resolve the missing satellites problem and to explain the apparently overdense hosts of low surface brightness galaxies predicted by CDM, but interest in SIDM mostly abated when it was shown that SIDM would produce strong effects in clusters of galaxies (among other reasons; see, e.g., Yoshida et al. 2000). Nevertheless, the range of models explored was relatively restricted, and Loeb & Weiner (2011) have recently argued that SIDM with a velocity-dependent cross section peaking at a velocity scale relevant for dwarfs retains the benefits of original SIDM models while avoids their drawbacks (see also Feng et al. 2009). Simulating structure formation in such a model would therefore be of significant interest.

#### 5.5 Missing Physics at $V < 50 \text{ km s}^{-1}$ ?

Ultimately, the structure of the Milky Way dwarfs must be understood as part of a full theory of galaxy formation that can explain the formation, evolution, and properties of all galaxies. It is therefore reasonable to ask whether the structural issues we have raised regarding MW dSphs are also seen in other systems of similar mass. Although observing galaxies at these masses over cosmological volumes is essentially impossible at present, THINGS (Walter et al. 2008) has observed 34 nearby galaxies ( $D < 15 \text{ Mpc}$ ) in HI with high spatial resolution. We use the results of Oh et al. (2011a,b), who performed a detailed mass modeling of seven low-mass THINGS galaxies, to compare the  $M_{\star} - V_{\text{infall}}$  relation for these isolated galaxies to the bright MW dSphs and to abundance matching expectations in Fig. 9.

Intriguingly, the THINGS data mostly lie above the abundance matching relation and its extrapolation to lower masses and provide a smooth transition from the abundance matching  $M_{\star} - V_{\text{infall}}$  relation at  $V_{\text{infall}} \gtrsim 75 \text{ km s}^{-1}$  to the regime of the MW dSphs at  $\sim 15 - 25 \text{ km s}^{-1}$  derived in this work. Simulations of isolated dwarf galaxies with masses comparable to the THINGS sample also fall above the abundance matching curve (Sawala et al. 2011). Note, however, that if the  $\Lambda$ CDM model is correct, and galaxies with  $V_{\text{infall}} \approx 40 \text{ km s}^{-1}$  typically have stellar masses of  $\sim 10^8 M_{\odot}$ , then current stellar mass functions are substantially underestimating the abundance of such galaxies. Alternatively, either most halos with  $V_{\text{infall}} \approx 40 \text{ km s}^{-1}$  host systems with much lower total stellar masses, or the abundance of halos at these masses is lower than what is predicted by  $\Lambda$ CDM. There are at least three additional lines of evi-

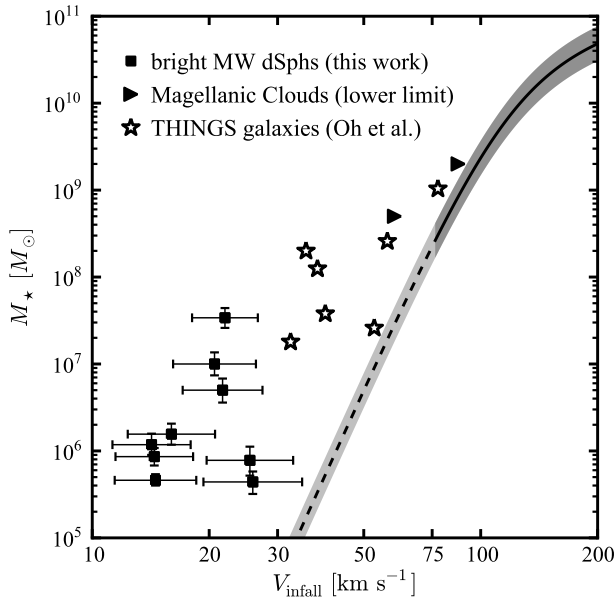


**Figure 9.** Inferred  $M_*(V_{\text{infall}})$  relation for bright MW dSphs (black squares with error bars, based on calculations in Sec. 4.1). The Magellanic Clouds (right-pointing triangles) are placed on the plot at their current values of  $V_{\text{flat}}$ , which is a lower limit to  $V_{\text{infall}}$ . Observations of low-mass field galaxies from THINGS (tabulated in [Oh et al. 2011a](#)) are plotted as open black stars. These galaxies all lie higher than the  $z = 0$  abundance matching relation (solid curve), as well as its extrapolation to lower  $V_{\text{infall}}$  (dashed curve), and the deviations are systematically larger at lower values of  $V_{\text{infall}}$ . The shaded region around the abundance matching relation shows a scatter of 0.2 dex in  $M_*$  at fixed  $V_{\text{infall}}$ , which is the upper limit allowed for massive halos  $V_{\text{infall}} \gtrsim 150 \text{ km s}^{-1}$  ([Guo et al. 2010](#); [Behroozi et al. 2010](#)).

dence arguing that isolated halos with  $V_{\text{circ}} \approx 50 \text{ km s}^{-1}$  do not match  $\Lambda$ CDM expectations:

- **HI observations:** The ALFALFA survey has performed a blind 21-cm emission line search over a wide area to look for neutral hydrogen in galaxies. [Papastergis et al. \(2011\)](#) have shown that while the velocity width function  $\Phi_w$  measured from ALFALFA agrees fairly well with  $\Lambda$ CDM predictions for massive galaxies, the observed number counts fall below those predicted by  $\Lambda$ CDM for  $w \lesssim 100 \text{ km s}^{-1}$  (corresponding approximately to  $V_{\text{max}} \lesssim 75 \text{ km s}^{-1}$ , assuming an average conversion of  $w_{50} = 0.75 V_{\text{max}}$ ). The discrepancy reaches a factor of  $\sim 8$  at  $w = 50 \text{ km s}^{-1}$  ( $V_{\text{max}} \approx 37 \text{ km s}^{-1}$ ) and becomes even worse at lower  $w$ .

- **Void galaxies:** [Tikhonov & Klypin \(2009\)](#) analyzed properties of voids in the Local Volume in comparison to theoretical predictions. They find that the abundance of void galaxies is over-predicted by a factor of  $\sim 10$  in  $\Lambda$ CDM at  $V_{\text{circ}} \approx 40 \text{ km s}^{-1}$ , and that the void size distribution is only reproduced if halos of  $V_{\text{circ}} \lesssim 40 \text{ km s}^{-1}$  do not host void galaxies (but see [Tinker & Conroy 2009](#)).

- **Damped Lyman- $\alpha$  systems:** The gaseous content of dark matter halos at  $z \sim 3$  can be probed by quasar absorption spectra. [Barnes & Haehnelt \(2009\)](#) have shown that many of the properties of damped Lyman- $\alpha$  systems can be understood in  $\Lambda$ CDM-based models. This success comes at the expense of requiring halos with  $V_{\text{circ}} \lesssim 50 \text{ km s}^{-1}$  to be

very baryon-poor. As noted in Section 3.3,  $50 \text{ km s}^{-1}$  is well above the photo-suppression scale at this redshift, indicating that reionization should not have caused such halos to lose a substantial amount of their baryons.

There are, of course, many potential sources of these disagreements, and the underlying  $\Lambda$ CDM theory is certainly not the most likely of these sources. A better understanding of feedback from star formation and its effects on halos of  $V_{\text{infall}} \lesssim 50 \text{ km s}^{-1}$  will be crucial, and may explain all of these apparent discrepancies, as well as other issues such as the central densities of low surface brightness galaxies (though see [Kuzio de Naray & Spekkens 2011](#) for arguments against baryonic physics explaining the density structure of these galaxies). It is imperative not to rely on plausibility arguments for the effects of feedback, but rather to understand whether realistic feedback models can actually produce dwarf spheroidal galaxies with properties akin to those seen in the Milky Way (as challenging as this may be!).

## 6 CONCLUSIONS

In this paper, we have expanded on the arguments of BBK, where we first showed that the bright satellites of the Milky Way apparently inhabit dark matter subhalos that are substantially less dense than the most massive subhalos from state-of-the-art  $\Lambda$ CDM simulations. Using subhalo profiles computed directly from the simulations rather than assuming subhalos are fit by NFW profiles, we have confirmed our previous result. Furthermore, we have now computed the most likely  $V_{\text{max}}$ ,  $V_{\text{infall}}$ , and  $M_{\text{infall}}$  values of the dwarf spheroidals using a likelihood analysis of the Aquarius data. This procedure predicts that all of the Milky Way dwarf spheroidals reside in halos with  $V_{\text{max}} \lesssim 25 \text{ km s}^{-1}$ , whereas more than ten subhalos per host halo are expected to have  $V_{\text{max}} > 25 \text{ km s}^{-1}$ .

This “massive failure” problem cannot be solved by placing the bright satellites in the subhalos with the largest values of  $V_{\text{max}}$  at infall or at the epoch of reionization: as discussed in Section 3.3 and shown in Figures 4 – 5, the missing subhalos are among the most massive at all previous epochs as well. Explaining this lack of galaxies in the expected massive subhalos is not natural in standard  $\Lambda$ CDM-based galaxy formation models: options include (1) a Milky Way halo that either is significantly deficient in massive subhalos, or is populated by subhalos with much lower concentrations than are typical; (2) stochasticity in galaxy formation at low masses, such that halo mass and luminosity have essentially no correlation; (3) strong baryonic feedback that reduces the central density of all massive subhalo by a large amount ( $\gtrsim 50\%$  reduction on scales of  $\sim 0.5 \text{ kpc}$ ).

We have argued above that these solutions all seem fairly unlikely as individual causes. It might be possible to apply them all at once: if the Milky Way halo mass sits at the low end of current constraints ( $\sim 10^{12} M_\odot$ ), and galaxy formation produces order unity scatter in  $M_*$  at fixed halo mass below  $\sim 50 \text{ km s}^{-1}$ , and baryonic feedback is able to alter the central densities of dark matter halos in a maximal way, then it may be possible to explain the low densities of the MW dSph galaxies. We find this combination somewhat implausible, but it is certainly worth exploring. A detailed comparison of the masses of M31 dSph galaxies

will be particularly useful in assessing the "rare Milky Way" hypothesis. Finally, if we do reject solutions (1)-(3), then we are left with the question of the nature of dark matter. Allowing for phenomenology such as self-interactions, decays, or non-negligible thermal velocities may explain the puzzles discussed here without destroying the many successes of cold dark matter models on large scales.

## ACKNOWLEDGMENTS

We thank Carlos Frenk, Fabio Governato, Martin Haehnelt, Amina Helmi, Juna Kollmeier, Andrey Kravtsov, Erik Tollerud, and Simon White for helpful and spirited discussions. The Aquarius Project is part of the programme of the Virgo Consortium for cosmological simulations; we thank the Aquarius collaboration for giving us access to their simulation data. MB-K thanks Takashi Okamoto for providing the data for  $M_c(z)$  plotted in Fig. 4. The Millennium and Millennium-II Simulation databases used in this paper were constructed as part of the activities of the German Astrophysical Virtual Observatory. MB-K acknowledges support from the Southern California Center for Galaxy Evolution, a multi-campus research program funded by the University of California Office of Research. JSB was supported by NSF AST-1009973; MK was supported by NASA grant NNX09AD09G.

## REFERENCES

- Ando, K. et al. 2011, PASJ, 63, 45  
 Barkana, R., & Loeb, A. 1999, ApJ, 523, 54  
 Barnes, L. A., & Haehnelt, M. G. 2009, MNRAS, 397, 511  
 Behroozi, P. S., Conroy, C., & Wechsler, R. H. 2010, ApJ, 717, 379  
 Benson, A. J., Frenk, C. S., Lacey, C. G., Baugh, C. M., & Cole, S. 2002, MNRAS, 333, 177  
 Besla, G., Kallivayalil, N., Hernquist, L., Robertson, B., Cox, T. J., van der Marel, R. P., & Alcock, C. 2007, ApJ, 668, 949  
 Blanton, M. R., Geha, M., & West, A. A. 2008, ApJ, 682, 861  
 Bovill, M. S., & Ricotti, M. 2009, ApJ, 693, 1859  
 —. 2011a, ApJ, 741, 17  
 —. 2011b, ApJ, 741, 18  
 Bovy, J., Hogg, D. W., & Rix, H.-W. 2009, ApJ, 704, 1704  
 Boyarsky, A., Lesgourgues, J., Ruchayskiy, O., & Viel, M. 2009, JCAP, 5, 12  
 Boylan-Kolchin, M., Besla, G., & Hernquist, L. 2011a, MNRAS, 414, 1560  
 Boylan-Kolchin, M., Bullock, J. S., & Kaplinghat, M. 2011b, MNRAS, 415, L40  
 Boylan-Kolchin, M., & Ma, C.-P. 2007, MNRAS, 374, 1227  
 Boylan-Kolchin, M., Springel, V., White, S. D. M., & Jenkins, A. 2010, MNRAS, 406, 896  
 Boylan-Kolchin, M., Springel, V., White, S. D. M., Jenkins, A., & Lemson, G. 2009, MNRAS, 398, 1150  
 Broderick, A. E., Chang, P., & Pfrommer, C. 2011, arXiv:1106.5494 [astro-ph]  
 Bryan, G. L., & Norman, M. L. 1998, ApJ, 495, 80  
 Bullock, J. S., Kravtsov, A. V., & Weinberg, D. H. 2000, ApJ, 539, 517  
 Busha, M. T., Alvarez, M. A., Wechsler, R. H., Abel, T., & Strigari, L. E. 2010, ApJ, 710, 408  
 Busha, M. T., Marshall, P. J., Wechsler, R. H., Klypin, A., & Primack, J. 2011, ApJ, 743, 40  
 Chang, P., Broderick, A. E., & Pfrommer, C. 2011, arXiv:1106.5504 [astro-ph]  
 Conroy, C., Wechsler, R. H., & Kravtsov, A. V. 2006, ApJ, 647, 201  
 Davé, R., Oppenheimer, B. D., & Finlator, K. 2011, MNRAS, 415, 11  
 De Lucia, G., Kauffmann, G., Springel, V., White, S. D. M., Lanzoni, B., Stoehr, F., Tormen, G., & Yoshida, N. 2004, MNRAS, 348, 333  
 Dehnen, W. 1993, MNRAS, 265, 250  
 Dekel, A., & Silk, J. 1986, ApJ, 303, 39  
 di Cintio, A., Knebe, A., Libeskind, N. I., Yepes, G., Gottlöber, S., & Hoffman, Y. 2011, MNRAS, 417, L74  
 Diemand, J., Kuhlen, M., Madau, P., Zemp, M., Moore, B., Potter, D., & Stadel, J. 2008, Nature, 454, 735  
 Efsthathiou, G. 1992, MNRAS, 256, 43P  
 Einasto, J. 1965, Trudy Inst. Astrofiz. Alma-Ata, 51, 87  
 Feng, J. L., Kaplinghat, M., Tu, H., & Yu, H.-B. 2009, JCAP, 7, 4  
 Font, A. S. et al. 2011, MNRAS, 417, 1260  
 Gao, L., Frenk, C. S., Boylan-Kolchin, M., Jenkins, A., Springel, V., & White, S. D. M. 2011, MNRAS, 410, 2309  
 Gao, L., Navarro, J. F., Cole, S., Frenk, C. S., White, S. D. M., Springel, V., Jenkins, A., & Neto, A. F. 2008, MNRAS, 387, 536  
 Gao, L., White, S. D. M., Jenkins, A., Stoehr, F., & Springel, V. 2004, MNRAS, 355, 819  
 Gnedin, N. Y. 2000, ApJ, 542, 535  
 Gnedin, N. Y., Tassis, K., & Kravtsov, A. V. 2009, ApJ, 697, 55  
 Gnedin, O. Y., Brown, W. R., Geller, M. J., & Kenyon, S. J. 2010, ApJ, 720, L108  
 Gnedin, O. Y., & Zhao, H. 2002, MNRAS, 333, 299  
 Governato, F. et al. 2010, Nature, 463, 203  
 Gunn, J. E., & Gott, J. R. I. 1972, ApJ, 176, 1  
 Guo, Q. et al. 2011, MNRAS, 413, 101  
 Guo, Q., White, S., Li, C., & Boylan-Kolchin, M. 2010, MNRAS, 404, 1111  
 Harris, J., & Zaritsky, D. 2006, AJ, 131, 2514  
 Hayashi, E., Navarro, J. F., Taylor, J. E., Stadel, J., & Quinn, T. 2003, ApJ, 584, 541  
 Hernquist, L. 1990, ApJ, 356, 359  
 Hoeft, M., Yepes, G., Gottlöber, S., & Springel, V. 2006, MNRAS, 371, 401  
 Jardel, J. R., & Gebhardt, K. 2012, ApJ, 746, 89  
 Kallivayalil, N., van der Marel, R. P., Alcock, C., Axelrod, T., Cook, K. H., Drake, A. J., & Geha, M. 2006, ApJ, 638, 772  
 Kirby, E. N., Martin, C. L., & Finlator, K. 2011, ApJ, 742, L25  
 Klypin, A., Kravtsov, A. V., Valenzuela, O., & Prada, F. 1999, ApJ, 522, 82  
 Klypin, A., Zhao, H., & Somerville, R. S. 2002, ApJ, 573, 597  
 Komatsu, E. et al. 2011, ApJS, 192, 18  
 Kopesov, S. et al. 2008, ApJ, 686, 279

- Koposov, S. E., Yoo, J., Rix, H., Weinberg, D. H., Macciò, A. V., & Escudé, J. M. 2009, *ApJ*, 696, 2179
- Kravtsov, A. 2010, *Advances in Astronomy*, 2010, 8
- Kravtsov, A. V., Berlind, A. A., Wechsler, R. H., Klypin, A. A., Gottlöber, S., Allgood, B., & Primack, J. R. 2004a, *ApJ*, 609, 35
- Kravtsov, A. V., Gnedin, O. Y., & Klypin, A. A. 2004b, *ApJ*, 609, 482
- Kuhlen, M. 2010, *Advances in Astronomy*, 2010
- Kuhlen, M., Krumholz, M., Madau, P., Smith, B., & Wise, J. 2011, *arXiv:1105.2376* [astro-ph]
- Kuzio de Naray, R., & Spekkens, K. 2011, *ApJ*, 741, L29
- Larson, R. B. 1974, *MNRAS*, 169, 229
- Li, C., & White, S. D. M. 2009, *MNRAS*, 398, 2177
- Li, Y., De Lucia, G., & Helmi, A. 2010, *MNRAS*, 401, 2036
- Li, Y.-S., & White, S. D. M. 2008, *MNRAS*, 384, 1459
- Loeb, A., & Weiner, N. 2011, *Physical Review Letters*, 106, 171302
- Lovell, M. R. et al. 2012, *MNRAS*, 420, 2318
- Ludlow, A. D., Navarro, J. F., White, S. D. M., Boylan-Kolchin, M., Springel, V., Jenkins, A., & Frenk, C. S. 2011, *MNRAS*, 415, 3895
- Lunnar, R., Vogelsberger, M., Frebel, A., Hernquist, L., Lidz, A., & Boylan-Kolchin, M. 2012, *ApJ*, 746, 109
- Macciò, A. V., & Fontanot, F. 2010, *MNRAS*, 404, L16
- Macciò, A. V., Kang, X., Fontanot, F., Somerville, R. S., Koposov, S., & Monaco, P. 2010, *MNRAS*, 402, 1995
- Madau, P., Diemand, J., & Kuhlen, M. 2008a, *ApJ*, 679, 1260
- Madau, P., Kuhlen, M., Diemand, J., Moore, B., Zemp, M., Potter, D., & Stadel, J. 2008b, *ApJ*, 689, L41
- Martin, C. L. 1999, *ApJ*, 513, 156
- Mateo, M. L. 1998, *ARA&A*, 36, 435
- McMillan, P. J. 2011, *MNRAS*, 414, 2446
- Merritt, D., Graham, A. W., Moore, B., Diemand, J., & Terzić, B. 2006, *AJ*, 132, 2685
- Moore, B., Ghigna, S., Governato, F., Lake, G., Quinn, T., Stadel, J., & Tozzi, P. 1999, *ApJ*, 524, L19
- Moster, B. P., Somerville, R. S., Maubetsch, C., van den Bosch, F. C., Macciò, A. V., Naab, T., & Oser, L. 2010, *ApJ*, 710, 903
- Muñoz, J. A., Madau, P., Loeb, A., & Diemand, J. 2009, *MNRAS*, 400, 1593
- Murray, N., Quataert, E., & Thompson, T. A. 2005, *ApJ*, 618, 569
- Navarro, J. F., Eke, V. R., & Frenk, C. S. 1996, *MNRAS*, 283, L72
- Navarro, J. F., Frenk, C. S., & White, S. D. M. 1997, *ApJ*, 490, 493
- Navarro, J. F. et al. 2004, *MNRAS*, 349, 1039
- Neistein, E., Li, C., Khochfar, S., Weinmann, S. M., Shankar, F., & Boylan-Kolchin, M. 2011, *MNRAS*, 416, 1486
- Oh, S.-H., Brook, C., Governato, F., Brinks, E., Mayer, L., de Blok, W. J. G., Brooks, A., & Walter, F. 2011a, *AJ*, 142, 24
- Oh, S.-H., de Blok, W. J. G., Brinks, E., Walter, F., & Kennicutt, Jr., R. C. 2011b, *AJ*, 141, 193
- Okamoto, T., & Frenk, C. S. 2009, *MNRAS*, 399, L174
- Okamoto, T., Gao, L., & Theuns, T. 2008, *MNRAS*, 390, 920
- Olsen, K. A. G., Zaritsky, D., Blum, R. D., Boyer, M. L., & Gordon, K. D. 2011, *ApJ*, 737, 29
- Papastergis, E., Martin, A. M., Giovanelli, R., & Haynes, M. P. 2011, *ApJ*, 739, 38
- Parry, O. H., Eke, V. R., Frenk, C. S., & Okamoto, T. 2012, *MNRAS*, 419, 3304
- Peñarrubia, J., McConnachie, A. W., & Navarro, J. F. 2008, *ApJ*, 672, 904
- Pfrommer, C., Chang, P., & Broderick, A. E. 2011, *arXiv:1106.5505* [astro-ph]
- Piatek, S., Pryor, C., & Olszewski, E. W. 2008, *AJ*, 135, 1024
- Polinsky, E., & Ricotti, M. 2011, *Phys. Rev. D*, 83, 043506
- Pontzen, A., & Governato, F. 2011, *arXiv:1106.0499* [astro-ph]
- Press, W. H., & Schechter, P. 1974, *ApJ*, 187, 425
- Rashkov, V., Madau, P., Kuhlen, M., & Diemand, J. 2012, *ApJ*, 745, 142
- Read, J. I., & Gilmore, G. 2005, *MNRAS*, 356, 107
- Reid, M. J. et al. 2009, *ApJ*, 700, 137
- Reines, A. E., Sivakoff, G. R., Johnson, K. E., & Brogan, C. L. 2011, *Nature*, 470, 66
- Ricotti, M., & Gnedin, N. Y. 2005, *ApJ*, 629, 259
- Robertson, B. E., & Kravtsov, A. V. 2008, *ApJ*, 680, 1083
- Sawala, T., Guo, Q., Scannapieco, C., Jenkins, A., & White, S. 2011, *MNRAS*, 413, 659
- Schechter, P. 1976, *ApJ*, 203, 297
- Shattow, G., & Loeb, A. 2009, *MNRAS*, 392, L21
- Somerville, R. S. 2002, *ApJ*, 572, L23
- Spergel, D. N., & Steinhardt, P. J. 2000, *Physical Review Letters*, 84, 3760
- Springel, V., & Hernquist, L. 2003, *MNRAS*, 339, 289
- Springel, V. et al. 2008, *MNRAS*, 391, 1685
- . 2005, *Nature*, 435, 629
- Springel, V., Yoshida, N., & White, S. D. M. 2001, *New Astronomy*, 6, 79
- Stanimirović, S., Staveley-Smith, L., & Jones, P. A. 2004, *ApJ*, 604, 176
- Stoehr, F., White, S. D. M., Tormen, G., & Springel, V. 2002, *MNRAS*, 335, L84
- Strigari, L. E., Bullock, J. S., & Kaplinghat, M. 2007a, *ApJ*, 657, L1
- Strigari, L. E., Bullock, J. S., Kaplinghat, M., Diemand, J., Kuhlen, M., & Madau, P. 2007b, *ApJ*, 669, 676
- Strigari, L. E., Bullock, J. S., Kaplinghat, M., Simon, J. D., Geha, M., Willman, B., & Walker, M. G. 2008, *Nature*, 454, 1096
- Strigari, L. E., Frenk, C. S., & White, S. D. M. 2010, *MNRAS*, 408, 2364
- Tassis, K., Kravtsov, A. V., & Gnedin, N. Y. 2008, *ApJ*, 672, 888
- Thomas, J. et al. 2011, *MNRAS*, 415, 545
- Thoul, A. A., & Weinberg, D. H. 1996, *ApJ*, 465, 608
- Tikhonov, A. V., & Klypin, A. 2009, *MNRAS*, 395, 1915
- Tinker, J. L., & Conroy, C. 2009, *ApJ*, 691, 633
- Tollerud, E. J., Boylan-Kolchin, M., Barton, E. J., Bullock, J. S., & Trinh, C. Q. 2011, *ApJ*, 738, 102
- Tollerud, E. J., Bullock, J. S., Strigari, L. E., & Willman, B. 2008, *ApJ*, 688, 277
- Tremaine, S., Richstone, D. O., Byun, Y., Dressler, A., Faber, S. M., Grillmair, C., Kormendy, J., & Lauer, T. R. 1994, *AJ*, 107, 634



- van den Bosch, F. C., Tormen, G., & Giocoli, C. 2005, MNRAS, 359, 1029
- Wadepuhl, M., & Springel, V. 2011, MNRAS, 410, 1975
- Walker, M. G., Mateo, M., Olszewski, E. W., Peñarrubia, J., Wyn Evans, N., & Gilmore, G. 2009, ApJ, 704, 1274
- Walter, F., Brinks, E., de Blok, W. J. G., Bigiel, F., Kenicutt, Jr., R. C., Thornley, M. D., & Leroy, A. 2008, AJ, 136, 2563
- Watkins, L. L., Evans, N. W., & An, J. H. 2010, MNRAS, 406, 264
- White, S. D. M., & Rees, M. J. 1978, MNRAS, 183, 341
- Wolf, J., Martinez, G. D., Bullock, J. S., Kaplinghat, M., Geha, M., Muñoz, R. R., Simon, J. D., & Avedo, F. F. 2010, MNRAS, 406, 1220
- Xue, X. X. et al. 2008, ApJ, 684, 1143
- Yang, X., Mo, H. J., van den Bosch, F. C., Zhang, Y., & Han, J. 2011, arXiv:1110.1420 [astro-ph]
- Yoshida, N., Springel, V., White, S. D. M., & Tormen, G. 2000, ApJ, 544, L87

## APPENDIX A: MASS PROFILES OF SIMULATED SUBHALOS

In BBK, we used the values of  $V_{\max}$  and  $r_{\max}$  computed in Springel et al. (2008) to construct NFW profiles for the Aquarius subhalos. While subhalos are generally well-fitted by NFW profiles in the aggregate, any individual subhalo may show (significant) deviations from the NFW profile specified by its  $\{V_{\max}, r_{\max}\}$  values. In this paper, therefore, we use the raw particle data to compute the circular velocity profiles of the Aquarius subhalos.

While using the raw particle data provides a much better estimate of the true mass profile of a subhalo than does the NFW assumption, we still must remember that we are interested in properties of subhalos on scales that are not much larger than the force resolution of the Aquarius simulations. Draco, for example, has a de-projected half-light radius of 291 pc (Wolf et al. 2010), while the Plummer-equivalent softening length  $\epsilon$  of the Aquarius simulations is 65 pc. The effect of force softening is to reduce the density on scales of  $\sim 3\epsilon$  or smaller (note that forces are Newtonian on scales larger than  $2.8\epsilon$ ). This will not affect differential quantities such as  $\rho(r)$  on larger scales, but will affect cumulative properties such as  $V_{\text{circ}}(r)$ , such that the measured mass is an underestimate of the true mass. For example, Font et al. (2011) find that the mass within 300 pc of the centers of Aquarius A-2 subhalos (the resolution level of the simulations used in this paper) is systematically underestimated by approximately 20% by comparing with the higher resolution Aquarius A-1 simulation.

We adopt the following procedure to correct for the effects of force softening. First, we fit the density profile of each subhalo with an Einasto profile on the range<sup>2</sup>  $[291 \text{ pc}, r_{\text{upper}}]$ , where  $r_{\text{upper}}$  is the smaller of 3 kpc or  $1.5 r_{\max}$ . This procedure typically results in very good fits: using the goodness-

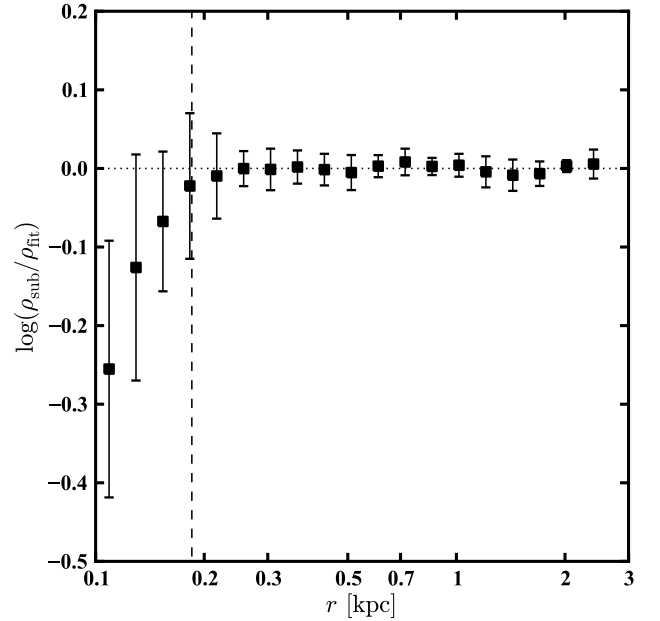


**Figure A1.** The difference between the measured subhalo density profiles and the best-fitting Einasto density profiles as a function of radius. The mean values (symbols), along with the standard deviations (error bars) based on the ten highest  $V_{\max}$  subhalos in the Aquarius B halo are plotted. The subhalos follow Einasto profiles (all with goodness-of-fit  $Q$  values of  $< 0.03$ ), with very small residual scatter, for  $r \gtrsim 250$  pc. On smaller scales, however, the measured profile falls below the Einasto fit because of gravitational softening. This causes an underestimate of  $V_{\text{circ}}(r)$  for  $r \lesssim 2.8\epsilon$  (forces for  $r > 2.8\epsilon$  are exactly Newtonian); this value is marked with a vertical dashed line.

of-fit measure

$$Q^2 = \frac{1}{N_{\text{bins}}} \sum_{i=1}^{N_{\text{bins}}} [\log \rho_{\text{subs}}(r_i) - \log \rho_{\text{model}}(r_i)]^2, \quad (\text{A1})$$

we find a median (mean)  $Q$  value of 0.057 (see also Fig. A1). We then use the best-fitting Einasto profile to model the density distribution for  $r < 291$  pc and the raw particle distribution for  $r \geq 291$  pc. The correction to  $V_{\text{circ}}$  from this procedure will be of decreasing importance with increasing  $r$ ; the correction is typically 5-10% at 291 pc. For a small number of subhalos (typically with low numbers of particles), the best-fitting Einasto profile has  $Q > 0.1$ . In this case, we opt to be conservative and do not apply any correction to the measured particle distribution. We also do not apply the correction for subhalos with  $r_{\max} < 500$  pc.

To assess the impact of this softening correction on our results, we re-ran the analysis from Section 4.1 without including the correction; Table A1 compares the two sets of results. The softening correction has minimal impact on the derived values of  $V_{\max}$ , with none of the dSphs changing by more than 5%.  $V_{\text{infall}}$  and  $M_{\text{infall}}$  are very stable as well: only Draco, the dSph with both the smallest half-light radius and largest inferred  $V_{\max}$ , is affected at the 9% level in  $V_{\text{infall}}$  (20% in  $M_{\text{infall}}$ ). Even these changes are much smaller than the errors on these values. We therefore conclude that our results are not driven by including (or excluding) the correction for gravitational softening.

<sup>2</sup> We choose 291 pc for the lower limit of our fits because this is the de-projected half-light radius of Draco, the most dense dSph in our bright sample.

**Table A1.** Effects of the softening correction on derived properties of the Milky Way dwarfs. For each dSph, we list two sets of numbers: the first row includes the softening correction, while the second row does not include the softening correction.

Name	$V_{\max}$ [km s <sup>-1</sup> ]	$V_{\text{infall}}$ [km s <sup>-1</sup> ]	$M_{\text{infall}}$ [ $M_{\odot}$ ]
Fornax	$17.8^{+0.7}_{-0.7}$	$22.0^{+4.7}_{-3.9}$	$7.4^{+6.1}_{-3.3} \times 10^8$
	$17.9^{+0.6}_{-0.6}$	$21.8^{+4.2}_{-3.5}$	$7.2^{+5.1}_{-3.0} \times 10^8$
Leo I	$16.4^{+2.3}_{-2.0}$	$20.6^{+5.7}_{-4.5}$	$5.6^{+6.8}_{-3.1} \times 10^8$
	$16.6^{+1.8}_{-1.6}$	$20.9^{+4.8}_{-3.9}$	$5.7^{+5.5}_{-2.8} \times 10^8$
Sculptor	$17.3^{+2.2}_{-2.0}$	$21.7^{+5.8}_{-4.6}$	$6.6^{+7.8}_{-3.6} \times 10^8$
	$17.6^{+1.7}_{-1.5}$	$22.1^{+4.5}_{-3.7}$	$6.9^{+6.0}_{-3.2} \times 10^8$
Leo II	$12.8^{+2.2}_{-1.9}$	$16.0^{+4.7}_{-3.6}$	$2.4^{+3.1}_{-1.4} \times 10^8$
	$13.2^{+2.1}_{-1.8}$	$16.7^{+4.3}_{-3.4}$	$2.7^{+3.3}_{-1.5} \times 10^8$
Sextans	$11.8^{+1.0}_{-0.9}$	$14.2^{+3.7}_{-2.9}$	$1.9^{+1.7}_{-0.9} \times 10^8$
	$11.9^{+0.9}_{-0.9}$	$14.3^{+3.7}_{-3.0}$	$1.9^{+1.7}_{-0.9} \times 10^8$
Carina	$11.4^{+1.1}_{-1.0}$	$14.4^{+3.7}_{-3.0}$	$1.8^{+1.8}_{-0.9} \times 10^8$
	$11.4^{+1.0}_{-0.9}$	$14.5^{+3.5}_{-2.8}$	$1.8^{+1.7}_{-0.9} \times 10^8$
Ursa Minor	$20.0^{+2.4}_{-2.2}$	$25.5^{+7.4}_{-5.8}$	$1.1^{+1.5}_{-0.6} \times 10^9$
	$20.3^{+2.2}_{-2.0}$	$26.1^{+7.4}_{-5.8}$	$1.2^{+1.6}_{-0.7} \times 10^9$
Canes Venatici I	$11.8^{+1.3}_{-1.2}$	$14.5^{+4.0}_{-3.1}$	$1.9^{+2.0}_{-1.0} \times 10^8$
	$11.8^{+1.3}_{-1.2}$	$14.6^{+4.0}_{-3.1}$	$1.9^{+2.0}_{-1.0} \times 10^8$
Draco	$20.5^{+4.8}_{-3.9}$	$25.9^{+8.8}_{-6.6}$	$1.2^{+2.0}_{-0.7} \times 10^9$
	$21.6^{+4.0}_{-3.4}$	$28.2^{+8.3}_{-6.4}$	$1.5^{+2.1}_{-0.9} \times 10^9$